GEOTHERMICA

COntrol SEISmicity and Manage Induced earthQuakes (COSEISMIQ)

Deliverable 3

Deliverable 3: The influence of physical parameters on the generation of induced seismicity
Hydro-geomechanical modeling

Authors: ETH : Dr. A.P. Rinaldi, V. Ritz
GeoEnergie Suisse AG : E. Colas, Dr. R. Castilla, Dr. P. Meier

Publication Date: 30.03.2020

The GEOTHERMICA is supported by the European Union's HORIZON 2020 programme for research, technological development and demonstration under grant agreement No 731117

Table of Contents

Abstract

Induced earthquakes in the context of geothermal project are an important tool to enhance the permeability and the productivity of reservoirs. However, felt and damaging induced earthquakes are a major threat to societal acceptance and regulatory license to operate. It is therefore very important to understand the mechanisms controlling induced seismicity. Geomechanical modeling is an essential tool, which allows to link seismological observations with physical processes governing induced seismicity, providing a framework for advanced interpretation strategies and decision support. The model is based on the Hellisheidi area in Iceland and especially the injection area Húsmúli, where the induced seismicity is high. The geomechanical model is based on studies of physical parameters presented in this report.

As soon as injection started in Húsmúli area, an important number of seismic events were recorded by the monitoring network and felt by the population. The analysis of the geometry, the spatial evolution of the seismicity, the geology and the hydraulic data allow to determine important physical parameters playing a role in the induced parameters. These parameters are integrated into the hybrid simulator TOUGH2-Seed to make the model more realistic and allow to understand the physical processes happening in the Húsmúli field. This report is a collaboration between Geo-Energie Suisse (Contexte to physical paramteter, chapter 1 to 5) and ETH (modelisation, chapter 6).

Our results show the implications of several parameters on the generation of induced seismicity. First, the structure and the tectonic background of the region will directly influence the seismic risk. In Húsmúli area, natural seismicity occurs and the presence of high instable faults make the area very favorable to generate induced seismicity. Then, the temperature also influences the friction and can define the slip behavior of the deformation. Above around 300 °C, the seismicity tends to be less frequent in the Húsmúli area. Below the 300°C Isotherm (e.g. below 2.2/3.4 km) seismicity decreases and below 2.8 km only 10% of the seismicity occurres. And finally, the hydraulic management is another important factor for the seismic risk, especially the flow rate (e.g. >400 l/s) and temperature of the injected fluid. Indeed, the hydraulic management will influence pressure changes in the reservoir and thus, will influence the generation of the seismicity.

1. Context

1.1. Enhanced geothermal system and induced seismicity

The EGS consists of extracting heat from the naturally fractured rocks, where the permeability and/or porosity is low. The hot target rock is stimulated by injection of fluid into the drilled well or by injection of chemical fluid, which dissolves certain minerals. Then, the running water is pumped and extracted via the production wells and then reinjected into the reservoir. Geothermal development in Switzerland driven by GES is based on EGS projects.

Hydraulic stimulation enhances or creates connections in reservoirs and generates controlled connectivity and fluid circulation without large pressure losses. Created connectivity between injection and production reservoir allows to keep a high pressure in the reservoir and thus a high production rate without reducing reservoir life (Tester *et al.,* 2006). These stimulations may induce seismicity, which can generate concerns among the local population.

Induced seismicity corresponds to the seismic events that cannot be made explicit by purely physical processes (such as tectonic or magmatic). Anthropogenic activity can create an early triggering of tectonic seismic events or also triggers earthquakes that would never have happened without human intervention (Duboeuf, 2018). Mechanisms involved in the anthropic seismicity are changes in the state of stress (magnitude and orientation), pore pressure changes and volume changes (Mc Garr *et al.,* 2002).

1.2. Control of seismic hazard: Advanced Traffic light systems

The occurrence of induced seismicity associated with hydraulic fracturing or injection over the last decades is pushing industries and government regulators to develop protocols to mitigate seismic hazards. The Traffic light systems is an approach to management of induced seismicity risks (Kao et al., 2016). TLS was developed as a tool for stimulation in enhanced geothermal systems and adapted for seismic risk mitigation, in the context of a variety of injection operations (Bommer *et al.,* 2006).

Therefore, TLS is used to guide drilling and stimulation monitoring. However, this tool works in real time to generate a reaction and cannot be used to forecast the evolution of seismicity. Thus, the aim is to improve induced seismicity prediction with predictive models based on statistics and geomechanical parameters.

Researchers developed a predictive model based on a combination of physical considerations and stochastic elements (Gischig & Wiemer, 2013; Goertz-Allmann & Wiemer, 2013; Karvounis *et al.,* 2014; Grigoli *et al.,* 2017; Broccardo *et al.,* 2019). This type of model is called Advanced Traffic Light Systems (ATLS). It includes a “seed model” and uses hydraulic behavior in the injection well, pressure diffusion, recorded seismicity, permeability behavior and differential stress based on the mean estimates of the in-situ stress field. The model is built with knowledge of the structure, with respect to the stress field and with usually a Mohr-Coulomb failure criterion. The output of the seed model is a time-dependent catalogue of seismic events including magnitude.

To develop a predictive model, it is important to understand the parameters controlling the induced seismicity. Therefore, studies of real examples allow a better understanding and could be applied to future projects. The WP3 of the COSEISMIQ project gives a better understanding of the influence of physical parameters (such as flow rate, injection/extraction duration, pore pressure changes, fracture distributions etc.) on the generation of induced seismicity. These physical parameters are implemented into the current development of the geomechanical modelling.

2. Hellisheidi geothermal field

The Hellisheidi Geothermal Field is operated by Reykjavik Energy (OR). 30 production wells are used to extract 500 kg/s of 180 °C steam and the installed capacity of the power plant is 303 MWe and 133 MWth. To maintain the production, it is necessary to manage re-injection of the extracted fluid to reduce the long-term pressure drop. Gráuhnúkar (2006) and Húsmúli (2011) represent the two most important injection zones and the total average injection rate is 1000 l/s (Hjörleifsdóttir, 2019) (Figure 1).

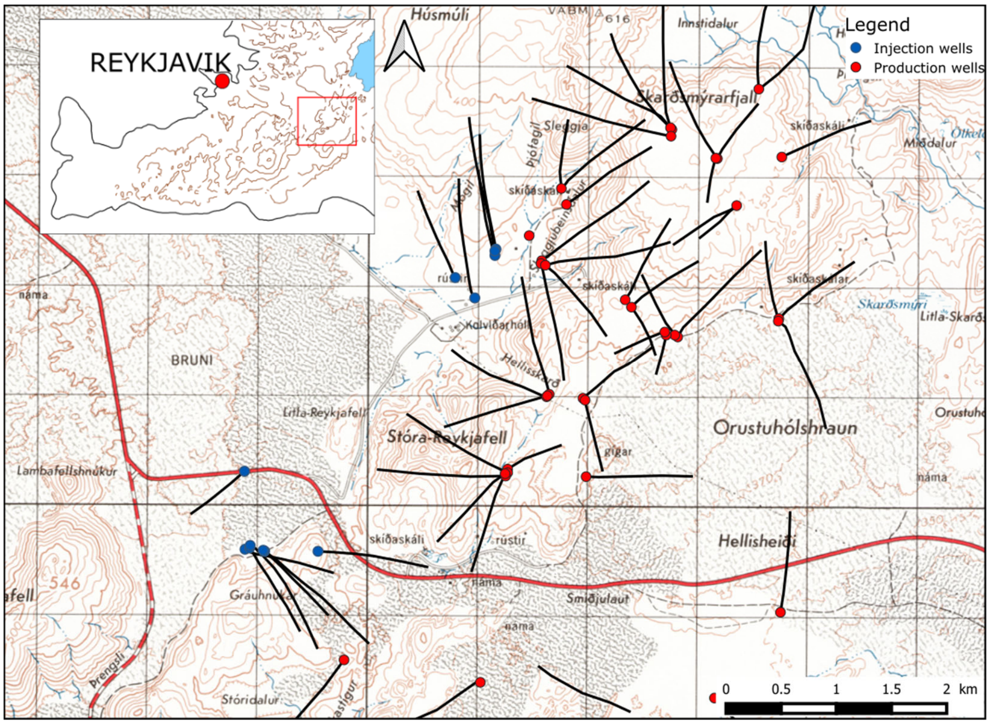

Figure 1: Map of the South of the Hengill area showing the Hellisheidi geothermal area with the two reinjection areas: the Húsmúli (North-West zone) and Gráuhnúkar (South-West zone) injection areas.

Gráuhnúkar was the first injection area drilled in the South-West of Hellisheidi field and is composed of six wells (from 700 to 1500 m depth TVD). An unexpected high temperature was found during drilling, up to around 300 °C which is interpreted as a separate up-flow zone. Induced seismicity in this area is relatively low compared to natural seismicity. Indeed, most of induced earthquakes are lower than ML 1.5 and the largest is ML 2.0. Moreover, induced seismicity did not immediately respond to injection. The first induced seismicity phase occurred in 2011 and then increased significantly from 2013 until today.

The injection in the Húsmúli area became fully operational in September 2011 with an injection rate of 550 l/s with an 8-bar pumping pressure. Immediately after the beginning of the drilling and then the onset of the injection in the Húsmúli area, an important number of seismic events were recorded by the monitoring network and felt by the population (Orkustofnun: National Energy Authority of Iceland; Gunnarsson, 2013). The induced seismicity remained high from September 2011 to May 2012 and then, it decreased as injection flow rates decreased.

Despite the proximity of the two injection areas (i.e. around 5 km apart), there is a clear difference of induced seismicity between the Húsmúli and the Gráuhnúkar areas. There is a difference in terms of frequency of the seismicity, magnitude and delay of the seismic response. These differences and their controlling factors are not yet fully understood. The high level of seismicity in the Húsmúli area during this period generated acceptance issues by the local population and affected the injection rate. To avoid a new Húsmúli seismic case, it is important to have a better understanding of the fluid circulation and factors triggering seismicity in the Húsmúli area.

The aim of this work driven by GES is to present factors playing a role in the induced seismicity. The study focuses on the link between the injection and the induced seismicity especially in the Húsmúli area to understand how fluid circulates in the Húsmúli reservoir.

3. Geological and tectonic settings

The Hellisheiði power plant is located in the Hengill volcanic system at the junction of three main tectonic features: The West Volcanic Zone (WVZ), the Reykjanes Volcanic Belt (RVB), and the South Iceland Seismic Zone (SISZ). The Húsmúli area is situated in the western border of the Hengill system. Five wells are active in this area among the seven wells (1000 m to 2100 m deep) drilled from 2008 to 2011, crossing the border faults of the Hengill system (N30°).

Húsmúli is part of the Hengill system and recovered by the Hengill formation composed of hyaloclastite (Sæmundsson, 1967, 1995; Sigvaldason, 2002; Loughlin, 2002), thick lava sequences occur during post-glacial eruption and Pleistocene (Saemundsson, 1967) and dykes representing as intrusive rocks from eruptive fissures with a directional trend in NE-SW (Franzson *et al.,* 2005). The hyaloclastic presents the principal formation of the system and formed by subglacial volcanic eruptions. The Hengill formation is based on a basaltic basement at 1600/1700 m depth (TVD) in the Húsmúli area (Figure 2).

Permeable zones were localized in the wells in Húsmúli based on the study of loss during the drilling and temperature evolution along the well.

Natural seismicity occurred in the Húsmúli area before the beginning of the injection in Hellisheiði (2006). Events occurred in the Húsmúli area during the seismic episode in 1995-1998 (Clifton *et al.,* 2002) with a maximum magnitude of ML 3.5.

Two major fault systems are present in this area. First, the Hengill fault system with major structures trending mostly in NE-SW direction (N30°) and confined into the Hengill volcanic zone (Appendix 5). These faults represent long structures visible on the surface and are preferential structures for magma intrusions, which can fill entirely the faults or only to a certain depth. The cartography of these dykes was carried out by geological log and surface mapping. Strong hydrothermal alteration is present along these faults, which characterizes a preferential up-flow path (Franzson *et al.,* 2005). The second fault set is associated to the SISZ related to the shift of the rift activity (Árnason & Magnússon, 2001). The SISZ is the main tectonically active structure in the Hengill system and is characterized by N0° to N10° structure (2 to 5 km long) and N60° to N80° structure (1 to 2 km long).

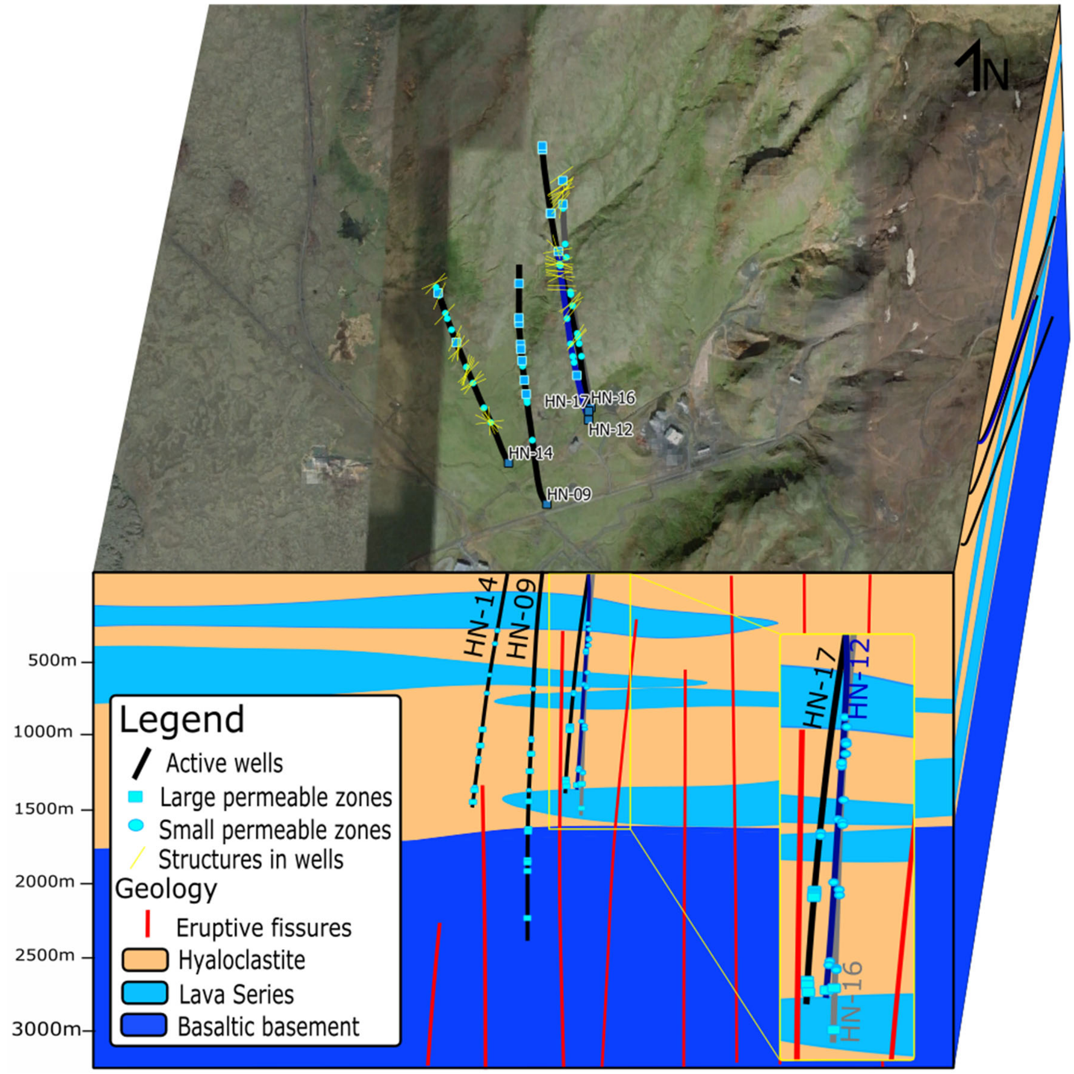

Figure 2: Conceptual geologic and structural 3D model in Húsmúli area. Yellow line show structures in wells (from drilling report, ISOR). Lithologic model is based on the Leapfrog© model of ISOR.

4. Description of the induced seismicity

The induced seismicity during operations of a geothermal field is a key element in the understanding of seismic hazard and changes in the reservoir. We focused our analysis during the intense seismic episode occurred between September 2011 to May 2012 and used the relocalized seismic catalogue of ISOR combining the seismic station of the SIL (national seismic station network) and a temporary seismic network deployed in 2011 and 2012 (Kristjánsdóttir, 2018). During this high induced seismicity period, around 40 000 events occurred in 8 months and more than 12 000 events only in September 2011. Activity decreased with the unexpected falling of injection levels. Despite a constant injection pressure, the injection level decreased from 2011 until now (From 550 l/s to 300 l/s). Analyses carried out during all the injection period (from 2011 to 2018) are based on the SIL catalog (national seismic network), where fewer seismic events are recorded (9100 events from 2011 to 2018).

4.1. Overview of the seismicity

The seismicity represents a cloud of 4 km (N-S) long and 3 km wide (E-W). Seismic events occurred first in a closed area around the wells and then they covered progressively a larger zone until they affected the entire area in a month. Seismic events occurred mainly along trends oriented N0°/10° and 30° (3.5 km long) and a general dip direction to the West. The Eastern limit of the seismicity seems to be well delimited following a N20°/30° orientation, while the western limit is characterized by a dense seismic cloud activated during April 2012 (Figure 3).

The depth of the seismicity is comprised from 1.5 km to 3.5 km depth TVD (±50 m). Most of these events are mainly concentrated in the basement between 1.7 km and 3 km depth TVD (±50 m). Two deep active structures (3.5-4 km) are visible on the E-W profile view and correspond to the two large eastern fault systems, while the western seismic cluster is only 2.5 km deep.

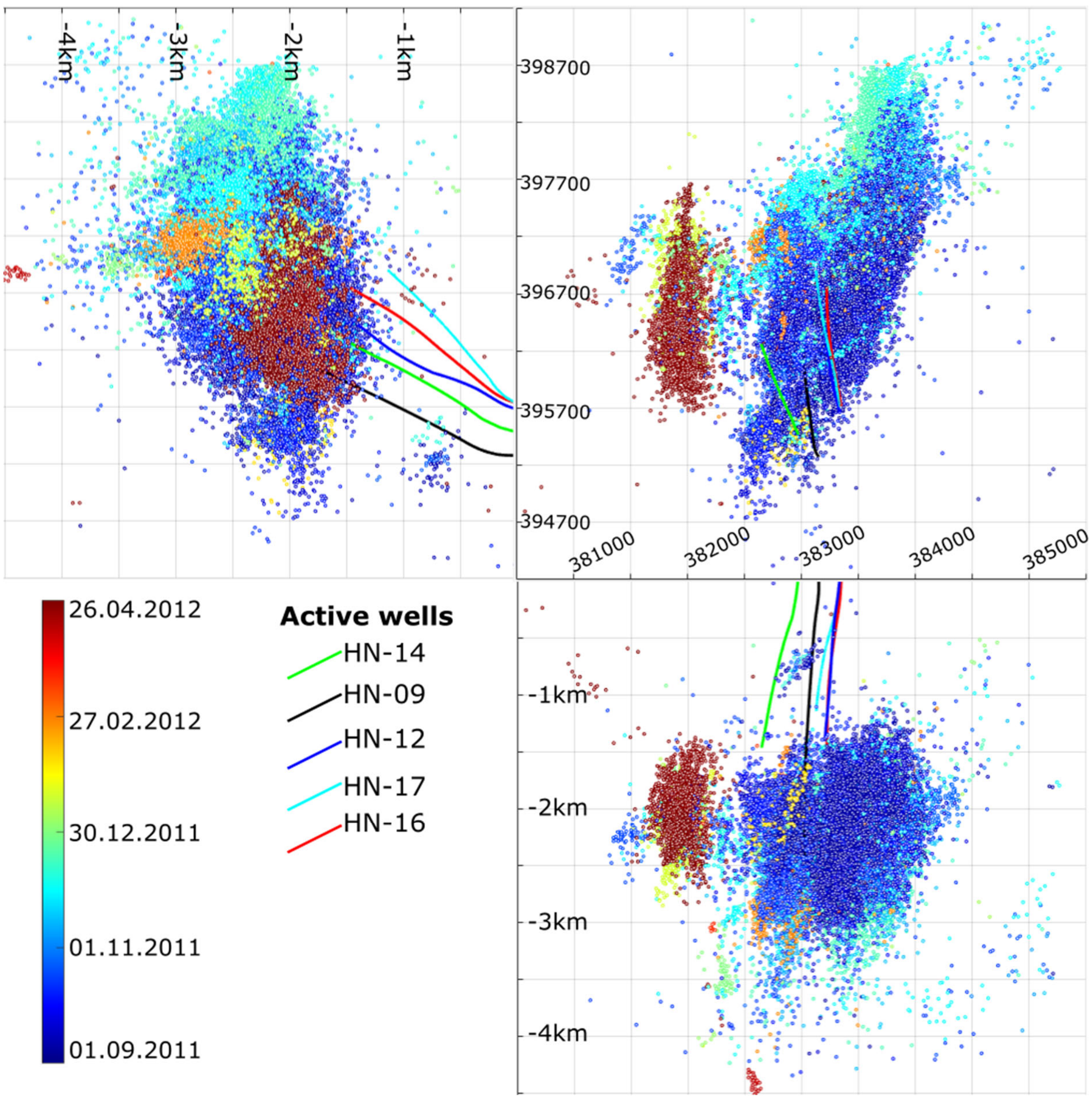

Figure 3: Map of the seismicity in the Húsmúli area from Sept. 2011 to May 2012 with North/South and West/East profile view (Seismic catalog: S. Kristjánsdóttir, 2018) (System ISN93).

4.2. Structure of the seismicity

Three main seismic clouds are visible on both map and profile view, in the Húsmúli area (Figure 3). These three clouds characterize dense fault network and represent elongate N0°/10° clouds. The eastern cloud represents a large zone with non-well defined N0/10° structures. This large cloud seems to highlight the presence of a dense and complex fault network along this structure and is well connected to the middle fault system, which is thinner and well defined. The western system has also a well-defined geometry and seems to evolve independently. An absence of seismicity is moreover clearly visible between the western fault system and the rest of the seismic cloud.

The 30° orientation is certainly associated with normal structures forming a graben in the Hengill system. These structures were well known before the onset of the injection and were the main target for injection wells as they represent the main pathways for fluid circulation (Aradottir *et al.,* 2012; Kristjánsson *et al.,* 2016; Tómasdóttir, 2018) (Appendix 9 and Appendix 10).

A further analysis of the induced seismicity during the period September 2011 to April 2012 allows to determine previously unknown fault network including faults oriented N0°-10° and dipping west and N40-60° faults. The N0-10° faults represent long strike-slip structure (2-3.5 km long) and the N40-60° represent smaller (300 m to 1 km) Riedel faults. The two orientations are characteristic of the SISZ fault orientation, which are a naturally active fault system (Figure 10, see part 5.2.1).

4.3. Spatio-temporal evolution of the seismicity

The Húsmúli area presents a clear relationship between drilling/injection rate and induced seismicity. The activation of previously unknown faults during the drilling phase and during injection highlights this link.

During the drilling phase, the seismicity was activated in the two eastern fault systems with an important induced seismicity period for the drilling of HN-14 (200 events, SIL catalog) and HN-17 (270 events, SIL catalog) (Appendix 15). Then, first induced events occurred during the injection phase and were also located along these two fault systems (Figure 3).

September to November 2011 represents the most active period in Húsmúli, when more than 27000 events occurred in only three months (Seismic catalog: S. Kristjánsdóttir, 2018). Then, the seismicity decreased, but remained strong during some important seismicity peaks such as the 17th of December 2011, the 18th of January 2012, the 24th of February or the end of April 2012 (Appendix 8).

During the first month of injection, the spatio-temporal evolution of induced earthquakes in the Húsmúli area shows a propagation along North/South and North-East/South-West faults. Then, one structure can be activated in a short period of time (hours or one day) followed by another structure with no apparent connection between them. The evolution of induced seismicity shows a pattern, where individual faults are turned on and off for short periods of time. The Figure 4 shows this seismic pattern clearly.

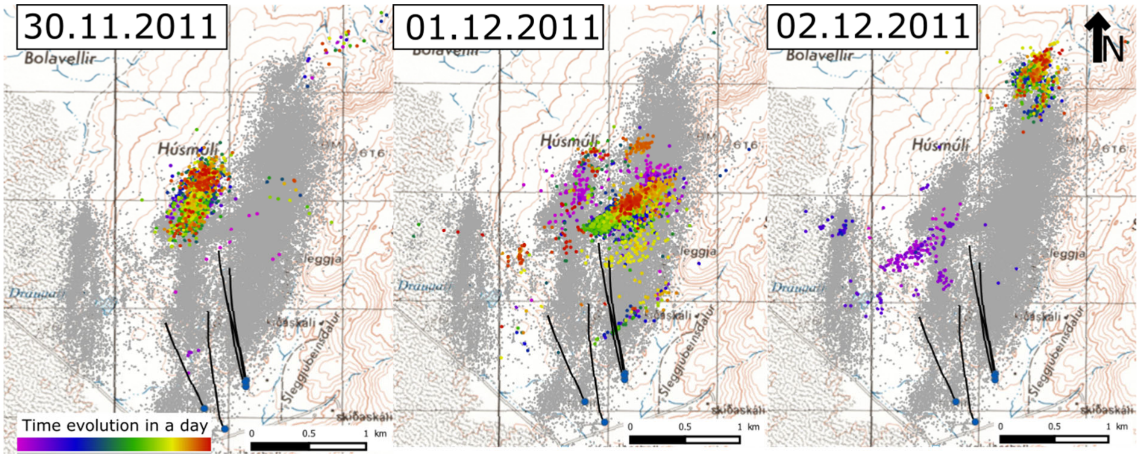

Figure 4: Evolution of the activation of faults during three days (from 30.11.2011 to the 02.12.2011). This pattern (colored dots) highlights a certain independence of the seismic dynamic.Grey dots show seismic events occurred from September 2011 to May 2012 (Seismic catalog: S. Kristjánsdóttir, 2018).

5. Influence of physical parameters

Geomechanical modeling is an essential tool, which allows to link seismological observable with physical processes governing induced seismicity, providing a framework for advanced interpretation strategies and decision support. To develop the geomechanical model we studied certain parameters, which can influence the generation of induced seismicity from the case of Húsmúli. The results of our analyses are described in this chapter.

These parameters allow to understand how natural or induced seismic events occur in the Hellisheidi area and then provide a better control of the induced seismicity. Moreover, this knowledge could guide the future of the exploration and drill plans in Hellisheidi area.

5.1. Temperature

The Hellisheiði area is characterized by a thermal anomaly associated to magmatic activity and fluid circulations along major Hengill faults. The temperature of rock formation influences frictional movements and then influences slip and seismic behavior. Temperature data are extracted from the Leapfrog© model (ISOR) at the initial state of the Húsmúli area. Temperature logs at the equilibrium are available only for the well HN-7 (Gráuhnúkar), HN-9 and HN-11 (Húsmúli)(Figure 5).

5.1.1. Observations of the temperature

Gráuhnúkar is characterized by a hydrothermal up-flow, which was not expected during the exploration phase. The maximum temperature in this area is more than 300 °C and reaches already 270 °C at 700 m depth SL (Figure 5).

Húsmúli area is located on the border of the Hengill system, where the reservoir temperature is cooler than in production zones. However, the thermal gradient in Húsmúli remains high and most of the injection wells reach 250 °C at 1500 m depth SL (Figure 5 & Figure 6).

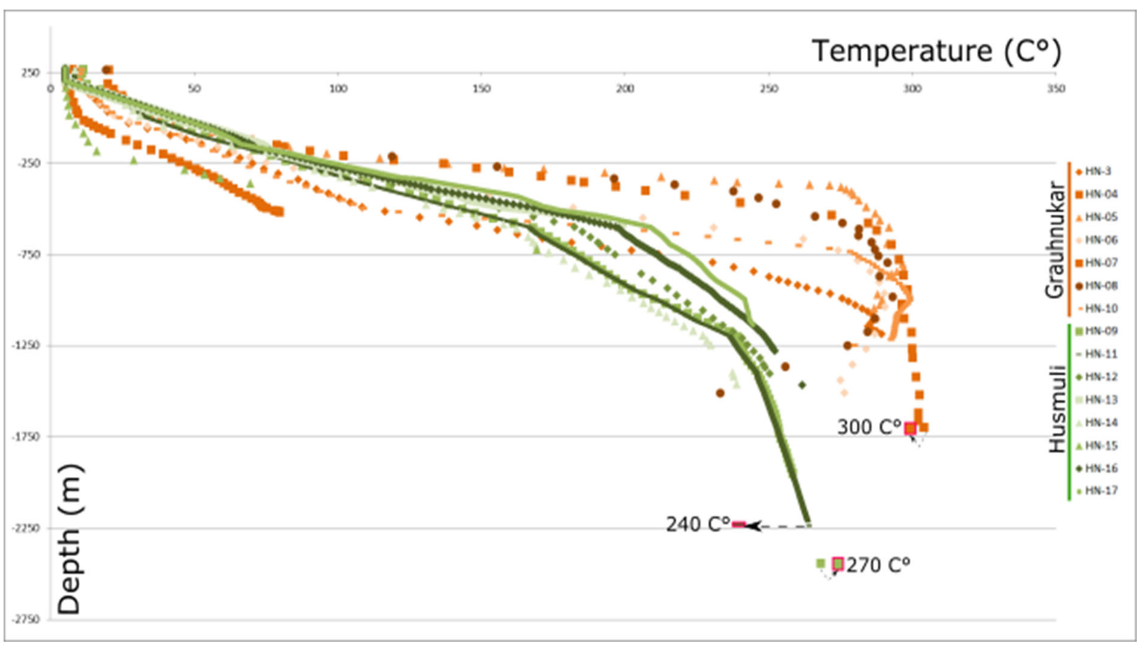

Figure 5: Log temperature of injection wells with sea level (SL): Húsmúli (green) and Gráuhnúkar (orange). Data from the temperature model of the Leapfrog model© (ISOR). Red squares represent data temperature from drilling reports for wells HN-7, HN-9 and HN-11.

The difference of 50 (at 1500 m depth) to 100 °C (at 1000 m depth) between Gráuhnúkar and Húsmúli could be a significant factor for whether or not induced seismicicy is triggeredIn the next section, we will discuss the different factors that play a role linked to temperature on induced seismicity.

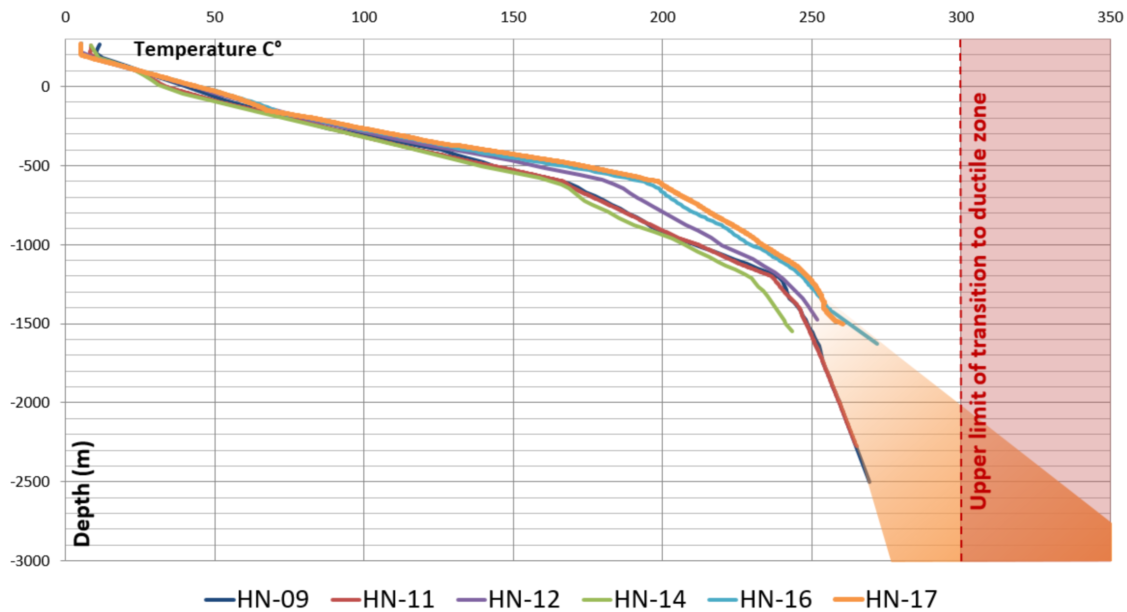

Figure 6 : Well temperature profiles (TVD). Data from the temperature model of the Leapfrog model© (ISOR) in the Húsmúli area and extrapolation of the geothermal gradient until 3000 m depth SL.

With an extrapolation of the geothermal gradient in the deeper part of the basement we can define a temperature range. The temperature might reach between 275 °C and more than 350 °C at 3000 m depth SL, which correlates with the brittle to ductile transition.

5.1.2. Introduction to the Brittle to Ductile Transition (BDT) and the Rate and State model

The temperature of rock formation influences frictional movements. The brittle to ductile transition (BDT) is a zone, where frictional characteristic of the media is changing and deformation occurs less likely with failure and more likely with ductility. This transition depends on the pressure, temperature and nature of rocks and is characterized by a reduction of seismicity below a certain depth. The BDT is directly linked to the frictional behaviour of the slip and the seismogenic layer, which is where 90% of the seismicity occurs in the crust.

The BDT is a transition zone taking into account three fields (Figure 7):

- The brittle field, which is the initial state: Field where seismic brittle failures occur,
- The semi-brittle field, which is the transition state: Field where shear failures and local plastic zones occur. Failures still occur, but slips are aseismic. The upper limit of this field corresponds to the base of the seismogenic layer,
- The ductile field, which is the final state: Field where the deformation is homogeneous.

Several studies try to find out temperature boundaries for different types of rock and in certain conditions. Results come from laboratory experiments with a pressure/temperature relationship similar to normal geothermal gradient (30 °C/km) (Blanpied *et al.,* 1995; Scholz, 1998; He *et al.,* 2007; Hartog *et al.,* 2012). From the analysis of the cutoff depth of the seismicity correlated to the geothermal gradient, Tryggvason et al., (2002) determined the end of the seismogenic layer in the south of Iceland at 665 °C ± 82 °C with a decrease of this temperature in the presence of water circulation by up to 150 °C (Scholz, 1988). From laboratory experiments Violay *et al*., (2012) defined this limit at for Icelandic basalt rocks at 550 °C ± 100 °C. In permeable media as in the Hengill system the depth of the beginning of ductility (i.e. the upper limit of the semi-brittle field) may be shallower due to the hydrothermal context and a second phase of crystallization in pore space (Adelinet *et al*., 2013).

The rate and state law is a model which predicts the friction depending on the displacement velocity. Others models exist to describe friction behavior. An earthquake occurs in a stick-slip frictional instability and when the frictional strength decreases.

The Rate and State model is function of the friction coefficient and the parameter a and b. If a slip is triggered (i.e. deformation occurring in the brittle and semi-brittle field), the combination of a and b will define if this slip is seismic or not. Parameter a and b is defined by the depth and the temperature and the rheology of the rock. When a-b is positive, the slip is aseismic (strengthening behavior) and is characterized by a constant evolution of the friction.

The strengthening behavior occurs in the near surface upper crust and defines the transition between the brittle to semi-brittle field. When a-b is negative, the slip is seismic (weakening behavior) and is characterized by sudden increases and decreases of the friction which create seismicity (Figure 7). The weakening behavior characterizes the seismogenic layer. In the brittle field, the a-b parameters increase until reaching a lowest value. This lowest value consists in the limit between the upper crust and the lower crust. Below this limit, a significant decrease of the seismicity is visible.

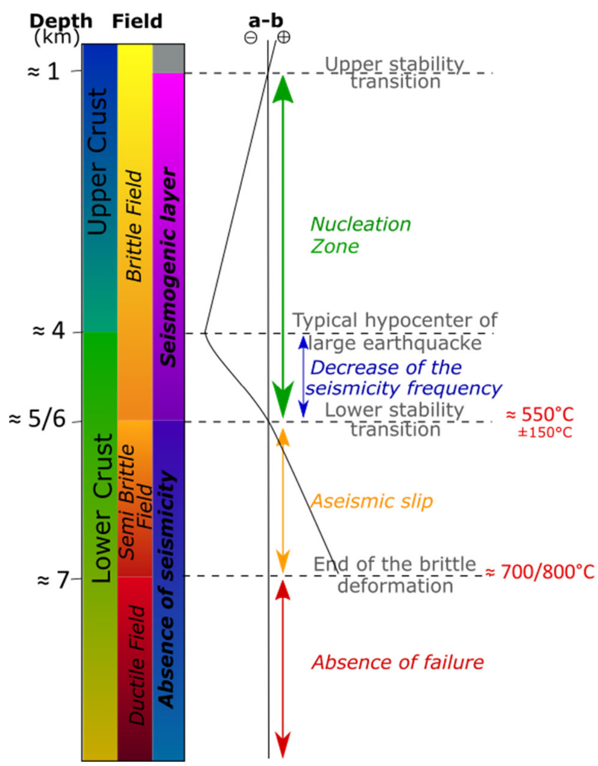

Figure 7: Representation of deformation field and slip behavior in the crust according to the BDT and the Rate and state model (Scholz, 1988; Tryggvason *et al.,* 2002; Fridleifsson & Elders, 2005; Violay *et al*., 2012). Boundaries (Depth and temperature) are applied to the Húsmúli area.

5.1.3. Seismogenic layer in Húsmúli area

From the temperature of the upper limit of the semi-brittle field, the base of the seismogenic layer is determined at 6 km (Tryggvason *et al.,*2002). Considering the volcanic context of Hengill system and the presence of fluid circulation, Violay *et al.,* (2012) defined this transition between 4 and 6 km depth. However, the definition of deformation fields is complex and plastic zones, characteristic of a ductile deformation, could be present at 3 km depth due to the presence of a second phase of crystallization in pore space (Adelinet *et al.,* 2013).

In Húsmúli area, above around 300°C (e.g. below 2.2 to 3.4 km depth TVD), the parameter a-b, that describes the slip behavior, tends to decrease and thus, seismic slip tends to be less frequent. Moreover, the bottom limit of the seismogenic layer described as the upper limit of the semi-brittle field is at around 5/6km depth TVD (550°C ±150°C) in the Húsmúli area which means that 90% of the seismic events occurred between Sept. 2011 and May 2012 are comprised between the surface and 2750 m depth and the deepest event occurred at 4800 m depth TVD. Below 3400 m depth (e.g. 1400 m above the deepest event), only 1% of the seismicity were triggered during the 2011/2012 period. On the contrary, for the same range (1400 m), between 1400 and 2800m depth, more than 90% of the seismicity occurred.

The boundary between brittle deformation and the semi-brittle deformation or between seismic slip and aseismic slip are complex and not precise. Regarding to temperature boundary and depth, the decrease of the number of seismic events below 2.8 km might not reflect the base of the seismogenic layer and may correspond to the beginning of a frictional change in the reservoir (at ≈300°C). This change is probably due to the transition between the upper and the lower crust. Below this transition the frequency of the earthquakes starts to decrease. Therefore, below 2.8 km, deformation is brittle but slips may tend to be aseismic.

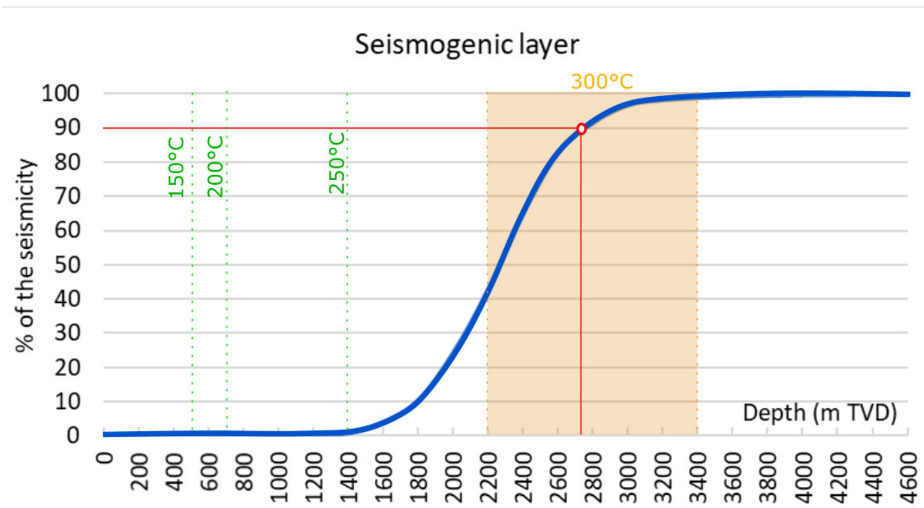

Figure 8: Repartition of the seismicity (Sept. 2011 to May 2012) along the depth TVD (Seismic catalog: S. Kristjánsdóttir, 2018). The orange square shows the possible range of the isotherm 300°C. This isotherm 300°C is present where the seismicity starting to decrease (frequency).

The high temperature present in Gráuhnúkar generates a shift upwards of the field boundaries and thus, likely cause the low level of induced seismicity. The difference of seismicity and temperature between the two injection areas highlights the importance of the consideration of the temperature in the generation of seismicity.

5.2. Structure and fault geometry

5.2.1. Hengill faults and Intrusive rocks

The Hengill system consist of a series of NE-SW fissure vents partially intruded with intrusive rocks. When these faults are not intruded, they represent large open faults. Tracer studies in the Húsmúli area showed a fluid circulation to the North-East with significant tracer recovery in the production area situated in the North-East of the Húsmúli area and suggests a main principal pathway for fluid circulation along these N30° faults (Kristjánsson *et al.,* 2016). This fluid circulation justifies the early propagation of the seismicity to the North/North-East during the beginning of the injection in Húsmúli.

However, the fillings by intrusive rocks of these faults consist in high density dykes. These intrusive rocks are linked to the volcanic activity of the Hengill system and consist in fine grained basalt, andesitic or rhyolitic intrusion (Franzson *et al.,* 2005). These dense rocks are characterized by a low permeability and porosity and play a role of barrier for fluid circulation.

Several N30° structures cross the Húsmúli area (Figure 9). The two western N30° faults were the main target for the drilling of injection wells. These faults are not intruded to more than 1.5 km depth while the two eastern N30° structures of Húsmúli are intruded by intrusive rock to the nearest surface. These eastern N30° structures bound the eastern seismic boundary of the Húsmúli area (Map, Figure 9). The correlation between the presence of these dykes and the seismic boundary suggest that these dykes are the eastern boundary of the Húsmúli area limiting fluid circulation and thus, the seismicity eastward.

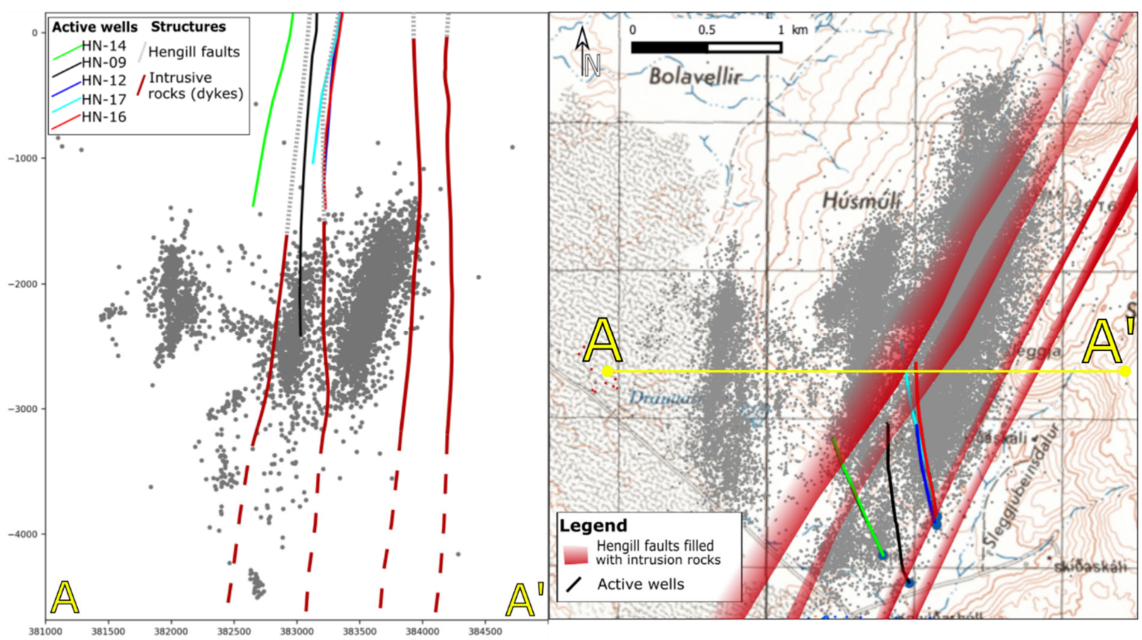

Figure 9: Presence of intrusive rocks along N30° Hengill faults. Structural map highlighting the presence of intrusive rocks (Right). Profile view of the N30°fault constraining the seismicity (grey dots) in the western side of the dykes, the dotted red line shows the extrapolation of the dykes in depth (Left). (Seismic catalog: Kristjánsdóttir, 2018)

5.2.2. Fault distribution

Added to the regional N30° trend representing the Hengill fissure swarm which is the rift orientation, the South Iceland Seismic Zone (SISZ) consists in a left-lateral active transform zone. The SISZ is the accommodation zone, which compensates the velocity delta of the spreading axis and has a left-lateral motion in direction creating Riedel faults oriented N0/20° (R) and N50/80°(R') (Khodayar & Franzson, 2007) (Appendix 5).

These orientations are well represented in the Húsmúli area (Figure 10). The three main clusters of seismicity in the area highlight three principal deformation zones oriented N10° with dextral motion. The two western N10° structures are characterized by a clear N10° fault while the eastern structure is complex with numerous Riedel left-lateral faults (R') oriented N50/80° and normal faults oriented N30°. The complex fault network explains the thickness of this seismic cluster.

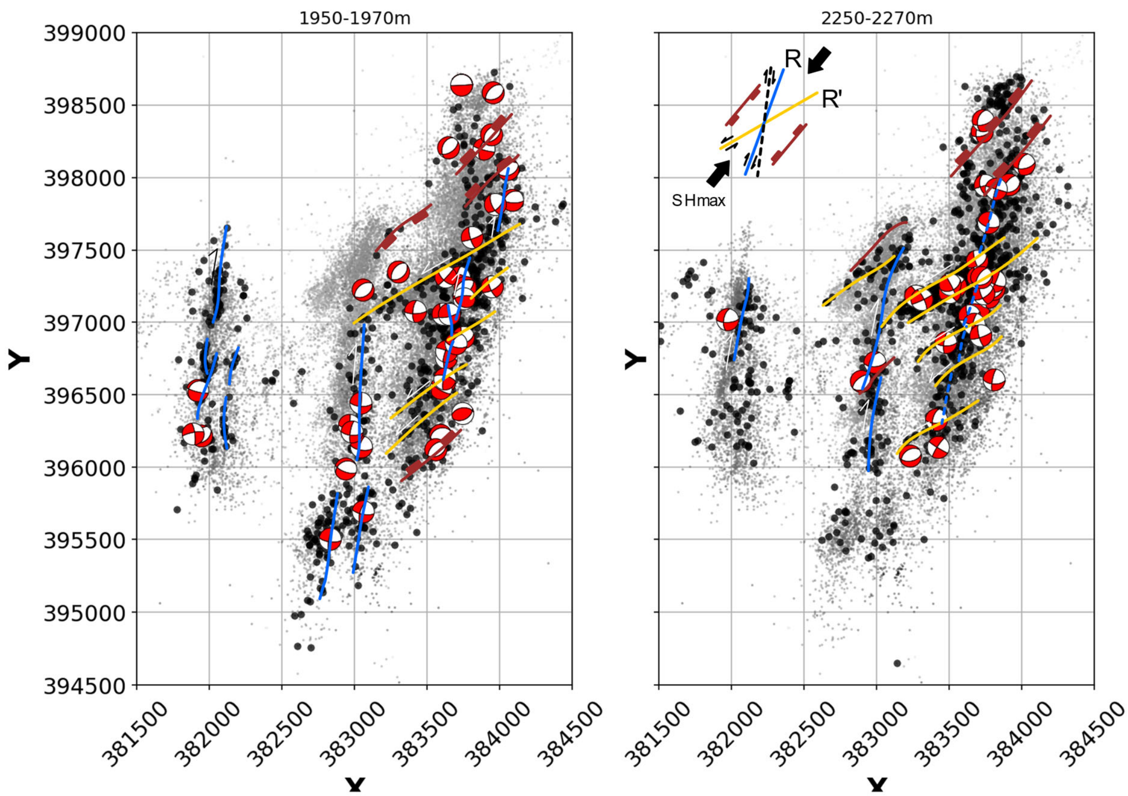

Figure 10: Map of structures highlighted by the seismicity and focal mechanisms in Húsmúli area. Focal mechanisms and seismicity are filtered according to the selected depth (1950/1970 m and 2250/2270 m TDV) with the representations of active structures (Seismic catalog: Kristjánsdóttir, 2018).

To understand if these structures are also present in the shallow part of the reservoir (in the hyaloclastite and the lava series), a comparison was carried out between seismic structure, structure in wells and surface fracture network (Figure 11). Considering the trajectory orientation of wells, some orientations may be more visible than others. For this reason, structures in wells are different according to each well, but the combination of the three wells structures distribution allows a good representation of the range of structures in the reservoir.

The two structure families (i.e. SISZ trend and Hengill trend) are represented in wells. An additional NW-SE orientation is strongly represented in HN-12 and also visible on the surface fracture network, but does not represent a preferential orientation for the induced seismicity.

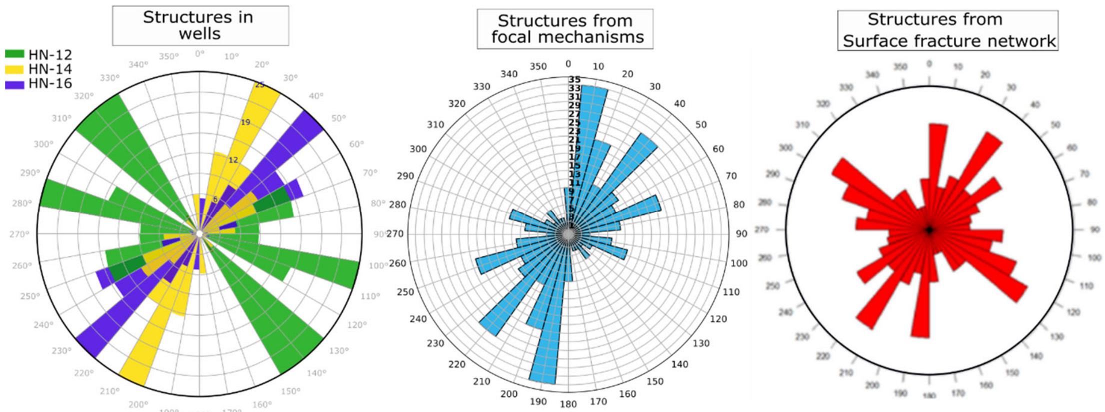

Figure 11: Fault orientations distribution along wells and highlighted by the seismicity (Structures in wells from drilling report, ISOR; Focal Mechanisms from Kristjánsdóttir, 2018; Structure from the surface fracture network, Khodayar, 2013).

In summary, the main structural orientations are:

- N10°/80°: The orientation of the 2 westernmost seismicity clouds observed in the ISOR catalogue. This direction represents the local principal deformation zone (PDZ) of a strike-slip system
- N20°/80: Riedel direction (R).
- N70°/80: Antithetic Riedel direction (R').
- N40°/60: Normal faults parallel to the maximum horizontal stress (SHmax).
- N120°/80: Observed only in borehole HN-12 and lineations on the surface. It might play the role of an antithetic P in a shear model.

5.3. Stress

5.3.1. Stresses in the Hengill area

The intense tectonic activity in Iceland implies that stresses can change with both space and time in association with particular, local events (e.g. major earthquakes, magmatic activity, increased hydrothermal circulation, etc.). For instance, Hensch et al. (2016) noticed a switch of stress state from normal to strike slip following two Mw=6.0 seismic events on May 29th 2008 in the Oluf region (15km SE of Hengill).

Most published works on the stress state in the study area focus on the South Iceland Seismic Zone (SISZ) (Lund & Slunga 1999; Keiding *et al.,* 2009 and Hensch *et al.,* 2016). Very few references analyze stresses on the axial zone of the Hengill fissure swarm were Húsmúli and Gráuhnúkar are located (Foulger, 1988; Batir, 2012) (Figure 12).

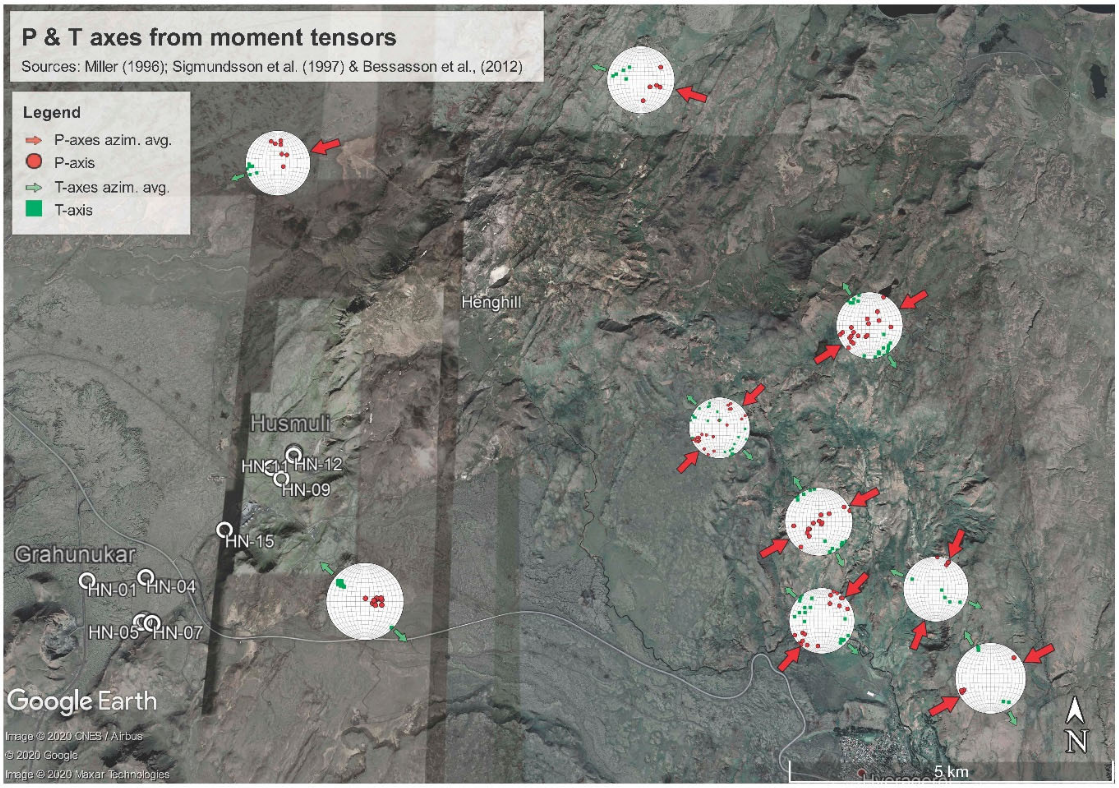

Figure 12: A database of 129 focal mechanisms was compiled from the literature (Miller 1996; Sigmundsson *et al.,* 1997; Bessasson *et al.,*2012). P and T axes from the focal mechanisms are mapped and used as a proxy for regional stress orientations.

A compilation of 129 focal mechanisms from the literature around the Hengill area is shown in Figure 12 (Miller 1996; Sigmundsson *et al.,* 1997; Bessasson *et al.,*2012). P and T axes from focal mechanisms are used as acceptable proxies for the preliminary analysis of the stress directions. The P and T ("Pressure" and "Tension" axes) are principal axes of the focal mechanism. Theoretically, the P axis represents the orientation of the largest negative P-wave amplitude, while the T axis is the orientation of the largest positive P-wave amplitude.

The compilation of P and T axes shows a marked difference between the SISZ to the east and the axial zone of the Hengill system to the west. P axes are oriented N20°-50° in the SISZ where a strike slip state is dominant. In contrast, P axes are markedly inclined to subvertical in the proximity of the Hengill system where crustal extension and accretion takes place. This stress scenario is of course valid only for the seismogenic zone and might change for depths shallower than 1.5-2 km.

The only published stress model derived from measurements in a borehole is the one reported in Batir *et al.* (2012). Three factors affected the results of the model proposed by Batir *et al.*:

1. Only one borehole was used to build the stress model (HN-16)
2. An inclined borehole was used: more assumptions need to be done to derive stress values and orientations when the borehole is inclined when compared to a vertical one.
3. No direct measurement of σ3: no mini-fracs or LOTs (Leakoff test) were available.
4. Unknown values of UCS (unconfined compressive strength): this is necessary to estimate stress magnitudes.

The results from Batir *et al,* (2012) point to a SHmax oriented around N26° similar to the orientation observed in the SISZ. The character of the stress state (normal, strike-slip or reverse) varied widely depending on the assumptions on the rock UCS but a general tendency was observed in depth. At 1000m TVD the stress state tends to be strike-slip while at 1400m TVD it transitions towards a normal state.

From a semi-regional point of view, we can conclude that the stress state near the Húsmúli and Gráuhnúkar injection fields is strongly influenced by the crustal spreading processes taking place in the Hengill system. It is therefore very likely that, at least at seismogenic depths, the stress field is characterized by EW to NW-SE extension.

5.3.2. Stresses in the Húsmúli injection field

Two main scenarios are tested and characterized in this study:

1. A homogenous stress state: By homogenous stress we mean a stress that doesn't change in space nor time and is constant all over the Húsmúli area. Three different stress states are included in this category:
    a. The Batir et al. (2012) deep stress state. This scenario corresponds to the analysis made on borehole measurements at 1400 m depth by Batir et al. (2012)
    b. A stress inversion (Michael, 1984) using 370 focal mechanisms in the Húsmúli area.
    c. Same as b but restricting the stress directions to be vertical and horizontal.
2. A heterogenous stress state: Is a stress state that changes in time and/or space.

5.3.2.1. Homogenous stress

As stated above, only one reference was available in the stress field at reservoir depths (Batir *et al.,* 2012). We have taken the results from this model as a reference for the stress state analysis carried out here despite the important uncertainties associated to it.

The other source for the generation of a homogenous stress state scenario is a set of 370 focal mechanisms recently derived for Húsmúli and made available by ISOR for this study (Kristjansdottir, unpublished data). This database covers the period from September 2nd, 2011 to April 25th 2012, corresponding to the period with highest injection rates in Húsmúli.

The main types of faulting in the database are strike-slip and normal. We have used the Kagan angle to visually differentiate both types of faulting in our analysis. The Kagan angle (Kagan, 1991) represents the rotation that should be applied to one focal mechanism to make it coincides with another one. By using a fixed focal mechanism as the reference and computing the Kagan angle between this reference and all the mechanisms in the database, we are able to differentiate the different kinds of faulting.

Figure 13 shows the database color-coded by the angle (Kagan angle) between each focal mechanism and a reference strike-slip double-couple (strike=90, dip=90, rake=0). Strike-slip (i.e. yellow, low Kagan angles), normal (red, high Kagan angles) and hybrid events (orange, intermediate Kagan angles) are distributed across the Húsmúli area with zones of higher concentrations for each type. Normal faults are dominant in the SE and SW corners while a high concentration of hybrid focal mechanisms can be seen near the northernmost tip of the database localizations.

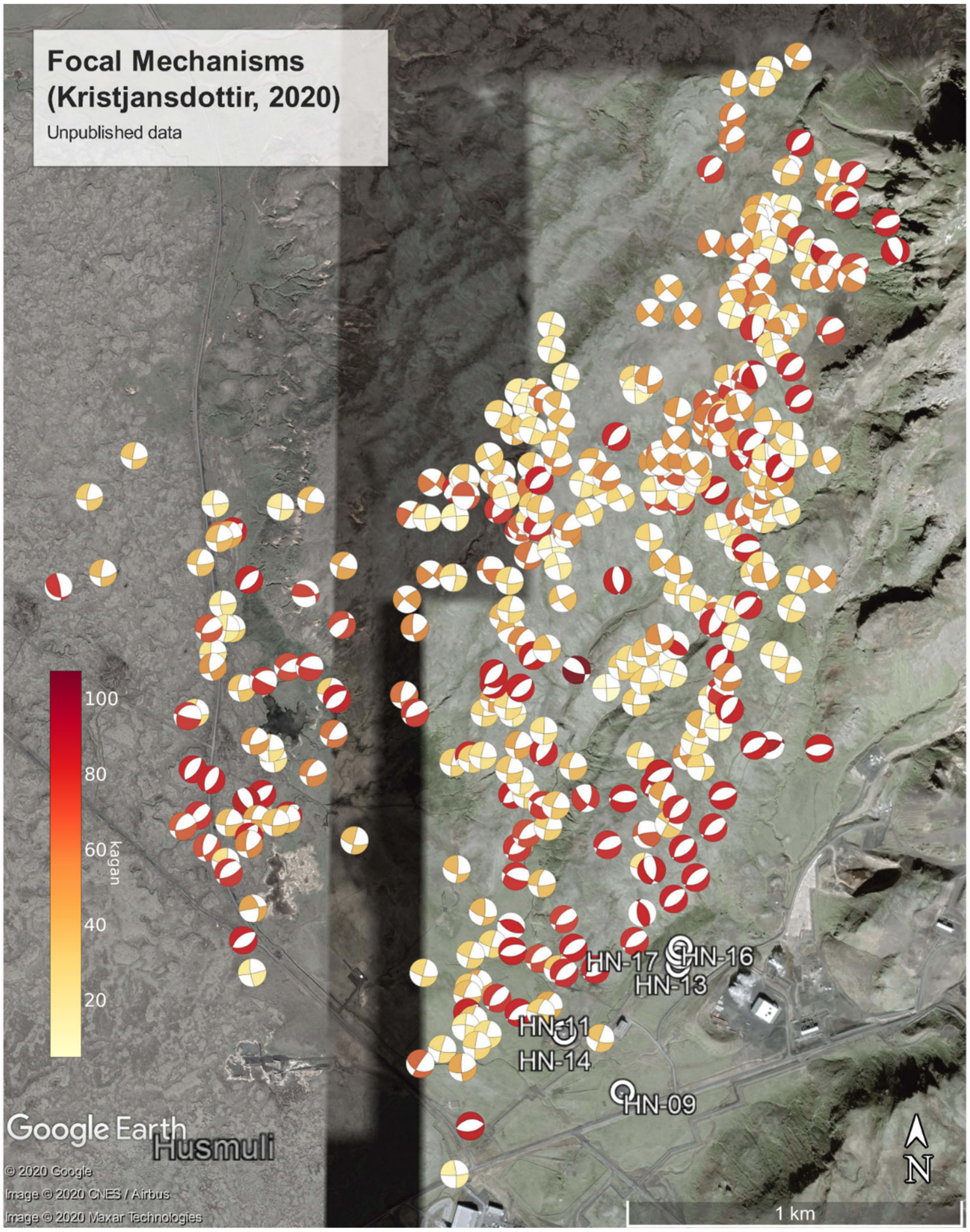

Figure 13. Focal mechanisms for the first seven months and a half of injection at Húsmúli. The color code corresponds to the Kagan angle between each focal mechanism and a reference double couple of strike=90°, dip=90° and rake=0°.

Two different stress inversions were carried using all the focal mechanisms included in the database. For both inversions, 5000 realisations were run using a bootstrap sampling of the faults in the focal mechanisms. The multiple sampling method (bootstrapping) is used to cope with the fact that two possible fault directions are possible for each focal mechanism and, in most cases, no a priori information is available to know which one actually moved during the seismic event.

A first inversion yields a transitional strike-slip to normal stress state (Figure 14). The maximum principal stress (σ1) is oriented N41° and dips 32°. A second inversion was run restricting the results to be "Andersonian" (principal stresses must be vertical and horizontal) (Figure 15). The trends are very similar but, in this case, the intermediate principal stress is vertical. The stress ratio is lower in the Andersonian stress state which implies the transitional strike-slip to normal condition is more marked.

Although these solutions are well constrained (i.e. there is little dispersion in the orientation of the principal axes) they do not succeed to predict slip along all faults in the focal mechanisms (i.e. the results are associated with rather high misfit angles). The misfit angle is the angle between the actual displacement vector along the fault, given by the focal mechanisms, and the theoretical displacement direction predicted by the stress state. A big misfit angle implies that the inverted stress does not explain very well the observed directions of displacement. This occurs often when a large range of different faults are used in a single inversion. In the present case, mean misfit angles of 24° (Figure 14) and 26° (Figure 15) result from using all the focal mechanisms for a single inversion. Despite this factor, we can use these results for the homogeneous stress state scenario in the whole Húsmúli area alternative to the one proposed by Batir *et al.* (2012). All the base case scenarios considered here are shown in Table 1.

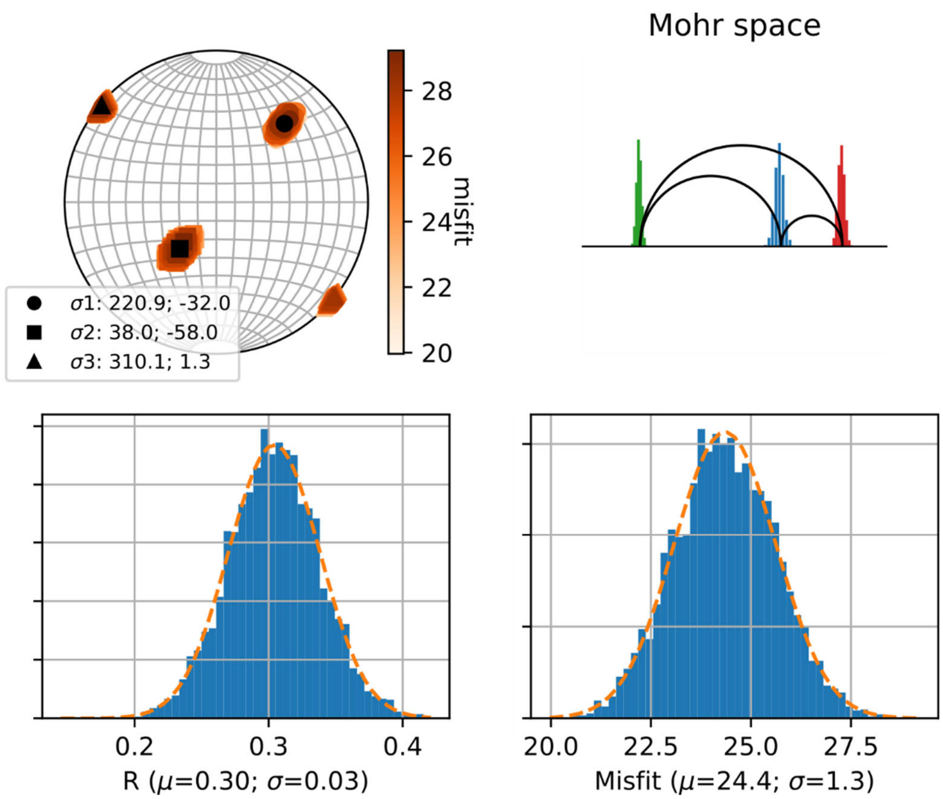

Figure 14. Stress inversion using all focal mechanisms in Húsmúli. The stereonet (upper left) shows all the solutions returned by the bootstrapping sampling method (see text). The Mohr circle shows the dispersion around mean values of the stress relative magnitudes. The lower row shows the histograms of the stress ratio (R) and the mean misfit angle for all 5000 realisations.

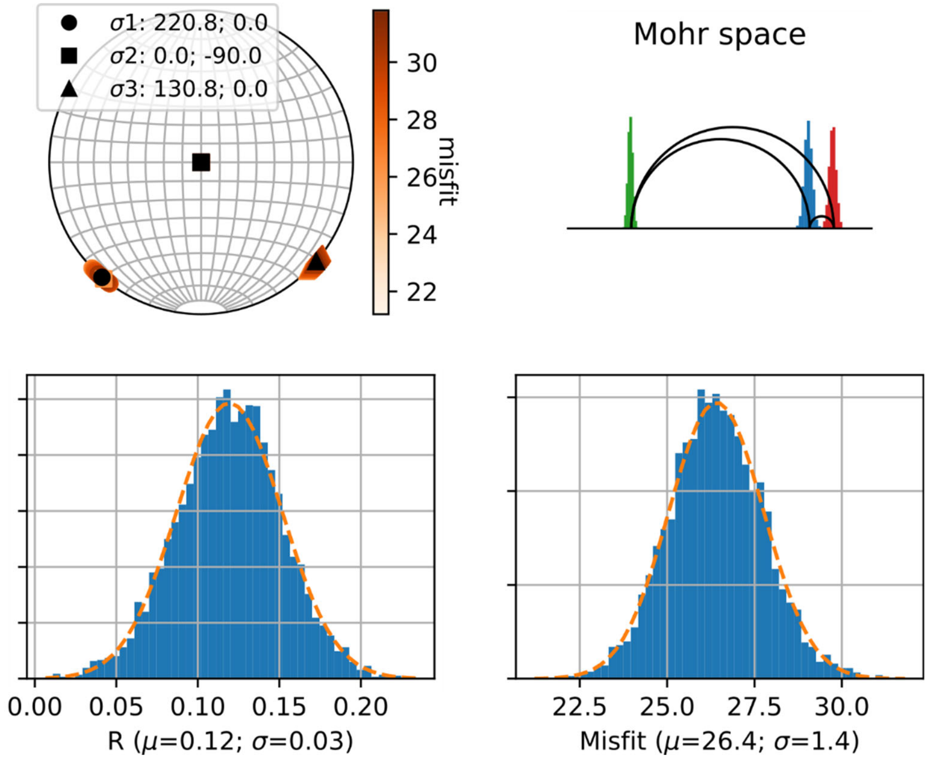

Figure 15. Stress inversion using all focal mechanisms in Húsmúli. In this case the inversion is restricted to vertical and horizontal principal stresses. See caption in Figure 14 for more information.

Table 1. Homogenous (constant) stress state models for the Húsmúli area

Source	Method	Depth (m)	Trend / Plunge			Magnitude (MPa)		
			SHmax			SHmax	Shmin	Sv
Batir et al., (2012)	Well (borehole breakouts)	1000	N26.6 ± 10° / 0°			30-38	12-25	25
		1400				25-35	19-23	35
This study	Inversion from focal mechanisms		σ1	σ2	σ3	R = (σ1 – σ2) / (σ1 - σ3)	Avg. Misfit angle	
	"Non-Andersonian"	1500-3000	N41±5°/ 32±7°	N208±5°/ 58±7°	N310±5°/ 1±2°	0.3±0.03	24±1	
	"Andersonian"		41±7°/0°	0°/90°	131±7°/0°	0.12±0.03	26.4±1.4	

5.3.2.2. Homogeneous stress and faults

The three scenarios of homogenous stress (i.e. Batir *et al.,* 2012 and inversion with all focal mechanisms) have been integrated with the main fault orientations identified and described in chapter 5.2 (Figure 16). All the calculations done here consider a hydrostatic in-situ fluid pressure (~10MPa/kmTVD). Multiple samples (n=5000) are generated around a mean stress state and a mean Mohr-Coulomb failure criterion and applied to known structural directions to estimate their reactivation potential (see Appendix 11 for details). The reactivation potential is described in terms of the additional fluid pressure needed to decrease the effective stress and reactivate a fault (Mildren et al, 2005). In Figure 16, the additional fluid pressure is simply the horizontal distance between the point clouds (representing the fault sets) and a yield criterion which is the black line (i.e. Mohr-Coulomb with friction coefficient = 0.4-0.6)

In all three stress scenarios and for 3 different depths (1500, 2000 and 2500 mTVD) faults oriented N120° are the less optimally oriented for reactivation. While most fault sets show slip are at the reactivation threshold, fault set N120° needs a minimum of 10MPa to be reactivated. This difference in the reactivation potential is certainly the main reason why the N120° fault set was only observed as fracture sets in one well (HN-12) and as fault traces in the surface but not as orientations reactivated after the onset of injection in Húsmúli.

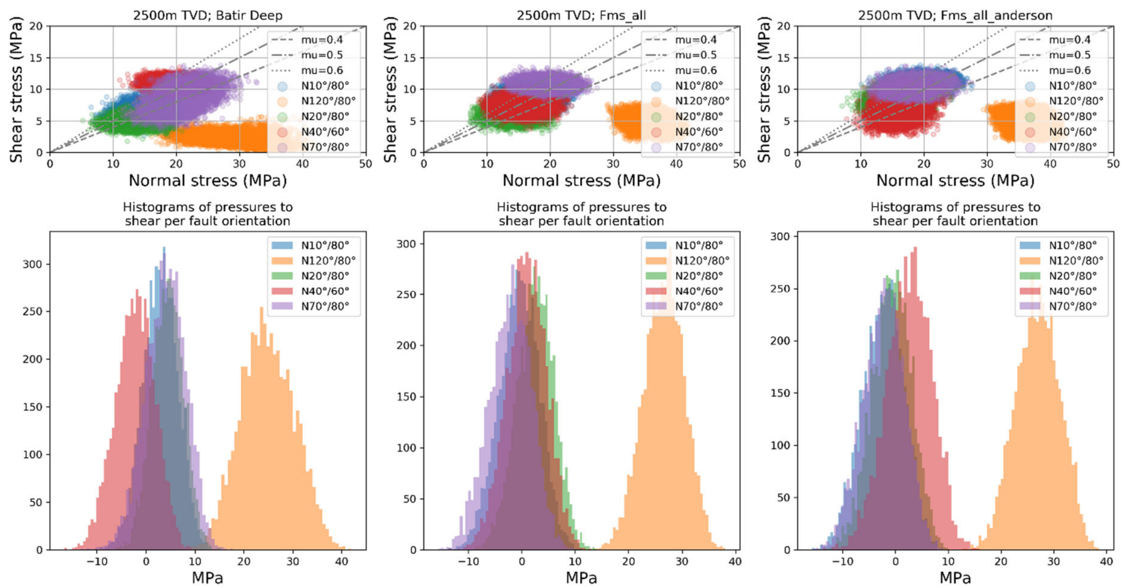

Figure 16. Reactivation potential of main structural directions in the Húsmúli area for the 3 homogenous stress scenarios listed in Table 1. 5000 realisations are run varying the parameters of both, the stress tensor and yield criteria around average values (see Appendix 11). Upper row: Normal vs. Shear stress for each fault family. Lower row: histograms of "slip stability" (necessary additional fluid pressure to shear) for each fault family. This figure corresponds to conditions at 2500 mTVD. For additional depths see Appendix 12 and Appendix 13.

In conclusion, for the base case stress state scenarios considered here, all fault sets, with the exception of N120°, are at the reactivation threshold.

5.3.2.3. Heterogenous stress state

A database of focal mechanisms, like the database for Húsmúli analysed here, contains information on faulting type and orientations. Significant changes in these parameters may be due to a number of reasons like changes in stress (tectonics, stress transfer, etc), fluid pressure modifications or dynamic triggering associated to other seismic events.

In the section that follows, we assume that changes in the pattern of fault reactivation are associated to stress changes. A detailed analysis of the focal mechanism database is carried out in order to test the hypothesis that stress changes occur during the injection.

The time distribution of focal mechanisms from Húsmúli shows periods where both strike-slip and normal faults are active at the same time (high and low Kagan angles; grey points in Figure 17), intercalated with periods where either strike-slip (low Kagan angle) or normal faults (high Kagan angle) are active (coloured points in Figure 17).

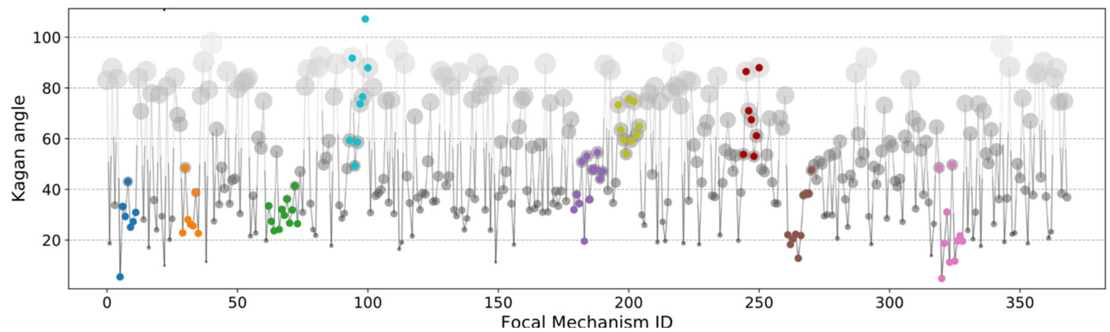

Figure 17. Evolution of focal mechanism types with time. High Kagan angles represent normal faults while low Kagan angles represent strike-slip faults. The horizontal axis represents a not-to-scale progression in time.

Nine subsets have been defined where fault reactivation is dominated by either strike-slip or normal fault types (Table 2, Figure 17, Figure 18 and Figure 19). These time periods between these subsets are characterized by the simultaneous reactivation of strike-slip and normal faults. The duration of each subset is variable and ranges from 43 mins to 7.7 days (Table 2).

Subsets tend to form tight clusters in space. This can be observed in the distribution of focal mechanisms for each set (Figure 18) but also when the same time limits are applied to the ISOR seismicity database (Figure 19).

Table 2. Subsets of focal mechanisms

Subset	Period			Kagan angle		Faulting	# of events
	start	end	duration	min	max		
Subset 1	2011-09-10 07:12	2011-09-10 07:55	0 days 00:43 hrs	5	43	Strike-slip	7
Subset 2	2011-09-13 01:40	2011-09-13 02:04	0 days 00:23 hrs	23	48	Strike-slip	7
Subset 3	2011-09-17 12:50	2011-09-21 21:25	4 days 08:34 hrs	24	41	Strike-slip	11
Subset 4	2011-09-29 05:55	2011-10-02 00:44	2 days 17:07 hrs	49	107	Normal	8
Subset 5	2011-10-22 07:31	2011-10-25 20:46	3 days 13:15 hrs	20	55	Strike-slip	12
Subset 6	2011-11-08 06:33	2011-11-16 00:10	7 days 17:36 hrs	54	76	Normal	9
Subset 7	2011-11-23 00:08	2011-11-23 13:20	0 days 13:11 hrs	53	88	Normal	7
Subset 8	2011-11-30 23:04	2011-12-01 00:06	0 days 01:01 hrs	13	47	Strike-slip	10
Subset 9	2012-02-24 18:26	2012-02-25 07:57	0 days 13:30 hrs	5	50	Strike-slip	10

The subsets of faulting type and their spatio-temporal organization show that the location and occurrence of induced seismicity is not completely random and, on the contrary, occurs in clusters. This means that those periods where only one kind of fault is reactivated are certainly associated to well defined processes (e.g. pressure diffusion, stress transfer, dynamic triggering, etc.).

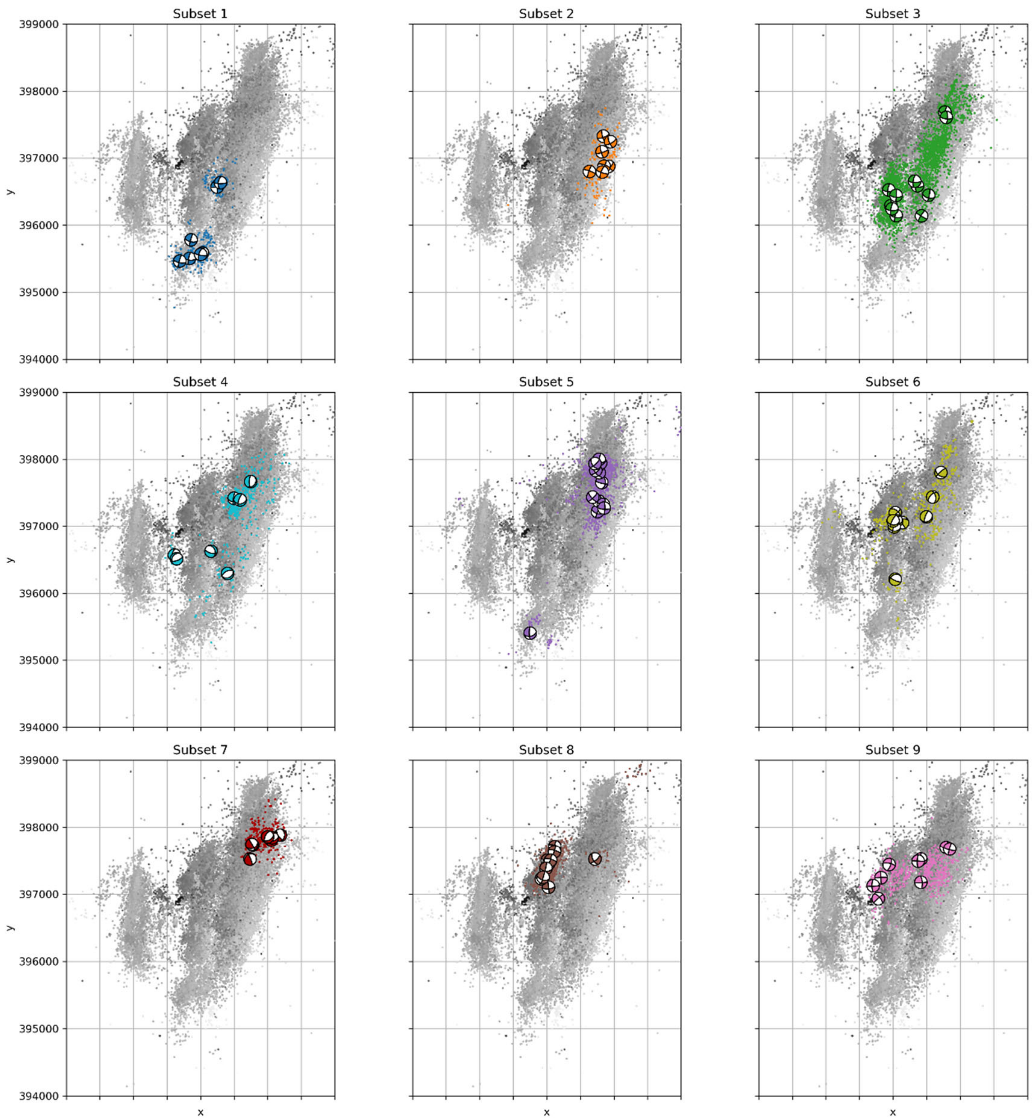

Figure 18. Subsets of focal mechanisms as described in Table 2 and Figure 17. The grey points correspond to all seismic events in the ISOR Húsmúli catalogue. The events corresponding to the time window defined by each subset have been coloured. Color code is the same as in Table 2.

Stress inversions carried out for each subset show the associated stress changes (Figure 19). The most important changes correspond to the plunges (inclination from the horizontal) of s1 and s2. Not surprisingly, the plunge of s1 tends to be higher for the subsets when normal faults are dominant (subsets 4, 6 and 7). Inversely, the plunge of s2 is higher when strike-slip is dominant. The value of the stress ratio "R" is also higher for subsets 4 and 7, meaning that the value of s2 gets closer to s3 in these periods of time and indicating a dominant normal stress state.

A stereonet representation of the stress changes is shown in Figure 20. It can be clearly seen that the plunge of s1 for subsets 4 and 7 is considerably higher than for the other subsets. The trend (horizontal angle from north) is rather constant for s1 and s3.

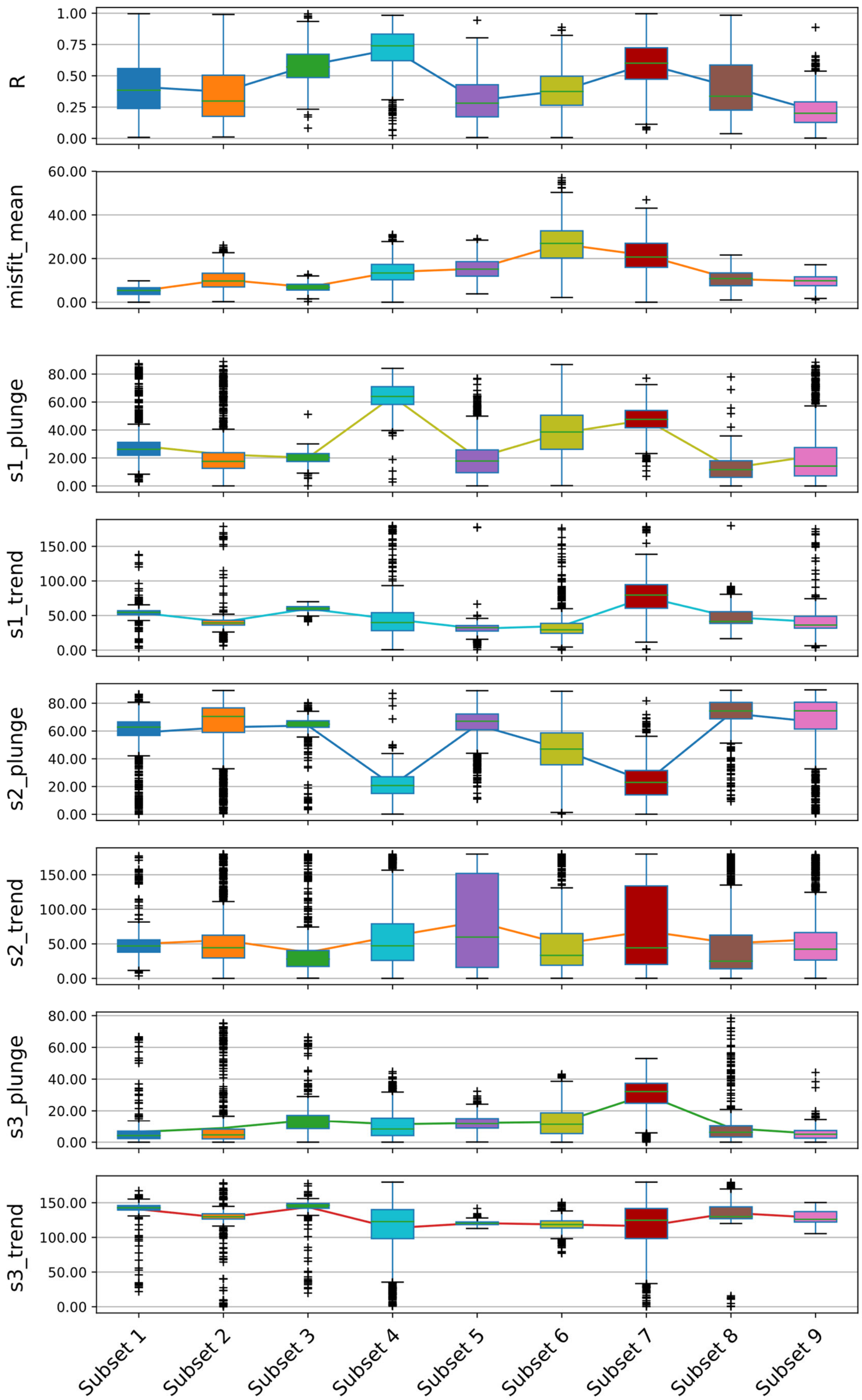

Figure 19. Boxplots of stress tensor parameters for each subset.

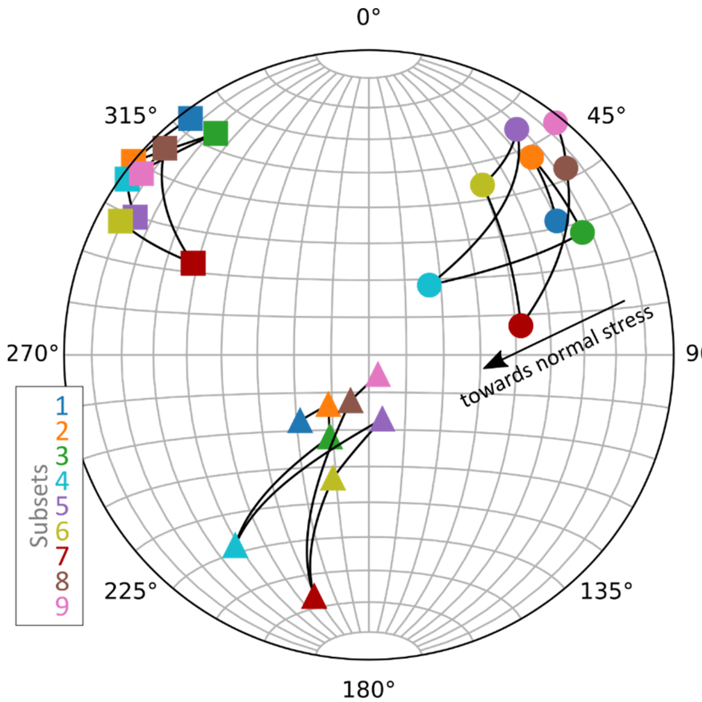

Figure 20. Stress changes associated to the reactivation pattern observed in the focal mechanisms. Cercles : σ1; Triangles: σ2; Squares: σ3

5.3.3. Homogenous vs. Heterogenous stress scenarios

The mean misfit angle was used to compare the homogenous and heterogenous (varying in time) stress states. For this purpose, a constant stress (inverted using all focal mechanisms in Húsmúli; Table 1) was applied to each subset described in Table 2. This was then compared to the mean misfit angle that results from applying the best fit stress state to each subset (Figure 21).

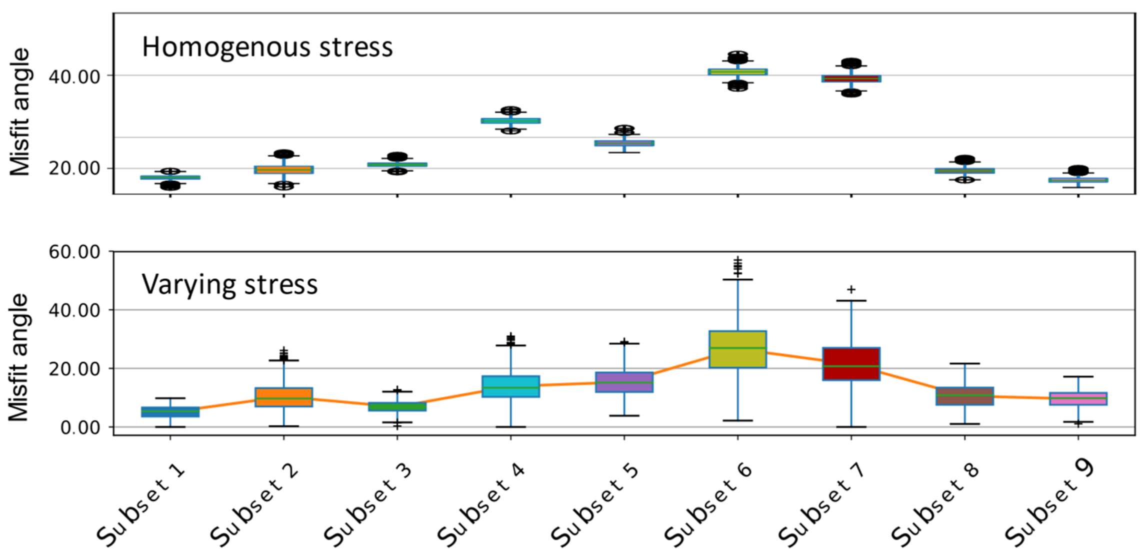

Figure 21. Comparison between homogenous and varying stresses with time.

The average misfit angles are significantly higher when a homogenous stress state is applied to all subsets. The values are especially high for subsets 4, 6 and 7 which correspond to those defined by dominant normal faulting.

This means that a homogenous stress state is not very good at explaining the activation pattern observed in the focal mechanism database. This is especially true for periods where normal faulting is predominant.

5.3.4. Conclusions on the stress state analysis

The stress state analysis carried out in the present study confirms some aspects already reported in the literature and shed news lights into some specific issues:

- The overall orientation of the stress state is fairly constant with one principal stress oriented in the axis NE-SW.
- The stress state is transitional between normal and strike-slip. The literature review suggests that at seismogenic depths, the stresses at Húsmúli tend to be dominantly normal.
- At least during the first 7½ months of injection in Húsmúli, periods dominated almost exclusively by normal or strike-slip faults intercalated with periods where a mixture of these two types of faulting where activated simultaneously.
- If stresses are considered as the main factor controlling fault reactivation then it is necessary to invoke changes in the local stress field with time as a constant-homogenous stress cannot explain these the variations of fault type.
- These changes in stresses might be triggered by a combination of factors:
    - Intense seismic activity (important magnitudes and/or high frequency of events) might induce stress shadows or zones of increased stresses in adjacent areas.
    - Increases in pore pressure in non-isotropic media (like fractured rocks) might induce non-isotropic changes in the stress tensor resulting in a rotation of the principal stresses.
- The changes of faulting type reactivation might also reflect other processes like dynamic triggering that were not investigated here and should not be ruled out.

5.4. Effect of the injection on the induced seismicity

The role played by fluids in the initiation of seismic rupture has been highlighted by numerous studies (Healy *et al.,* 1968; Sibson, 1973; Cornet *et al.,* 1997; Ellsworth, 2013; Bao & Eaton, 2016). In the 1960s, a cause-and-effect relationship was established between fluid injection and induced seismicity (Healy *et al.,* 1968).

Injection of fluid at high pressure into a reservoir reduces the effective stress while shear stress stays constant. If the Mohr circle reaches the failure envelope, an earthquake can occur and generates a release of accumulated energy. This release generates a stress drop until reach a new state of stability.

5.4.1. Influence of the injection rate on the seismicity

Onset of the injection and onset of the seismicity

There is a clear correlation between the beginning of the drilling (Appendix 15) or during the onset of the injection and the sudden increase of the seismicity in the Húsmúli area. The analysis of the evolution of the seismicity from 2000 to 2018 is based on the SIL catalog. From 2000 to 2008, only 165 events with an average of 18 events per year (SIL catalog).

During the drilling from 2008 to 2011, more than 770 events occurred and especially during the drilling of HN-14 (200 events) and HN-17 (270 events). Injection in the Húsmúli area began in September 2011 with a maximum rate of 600l/s with a constant well head pressure of 8bars. The onset of the injection represents a clear increase of seismicity (Figure 22) the first day and then 5 days later. More than 3400 events (≈35 000 events with the seismic catalog of Kristjánsdóttir, 2018) occurred in four months. The impact of the injection in visible all along the injection period with an average of 1150 events per year.

The number of seismic events highly increased since the beginning of the exploitation in the Húsmúli area. However, the number of large earthquakes (magnitude >3) remained similar with 4 earthquakes between 1995 and 2010 (Magnitude max 4.64) and 7 earthquakes between 2011 and 2018 (magnitude max 3.98).

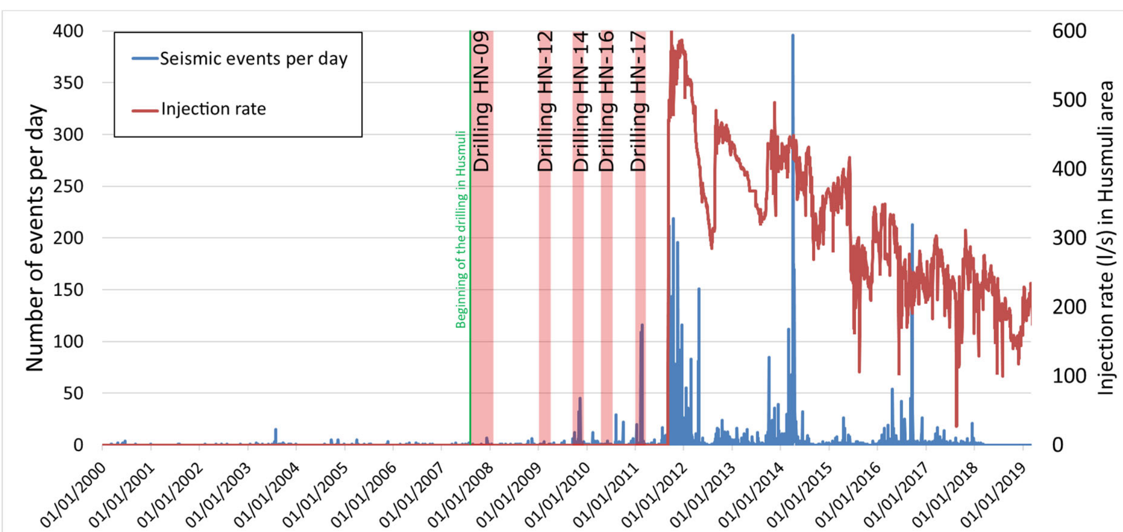

Figure 22: Evolution of the seismicity and the injection rate along time (Seismic catalog SIL Network).

Effect of the injection rate on the number of seismic events

From September 2011, three seismic episodes are recorded with high frequency level of seismicity: September 2011 to April 2012, October 2013 to April 2014 and April 2016 to December 2016 but the number of events per episode was decreasing with time (respectively 4464, 2220, 1139 events according to the SIL Catalog). After a first seismic episode responding to the onset of the injection (September 2011 to May 2012), the seismicity decreased with the injection rate.

In a large scale, the influence of the injection on the seismicity is clearly visible with a decrease of the frequency of seismic events with a decrease of the injection rate. The Figure 23 shows clearly an increase of the number of events per week linked to the increase of the injection rate (average injection rate per week). When the average injection rate is above 400 l/s, 21 weeks are characterized by more than 100 events per week against 3 weeks for an injection rate below 400l/s. Moreover, above 500 l/s every week is associated to seismic activity (Figure 23). This boundary for a rate 400 l/s may represent an upper limit of the injection rate to avoid high levels of seismic activity (frequency). The dependence of the injection rate on the number of seismic events is also visible at different scales such as per month (Appendix 18) and per six months (Appendix 19).

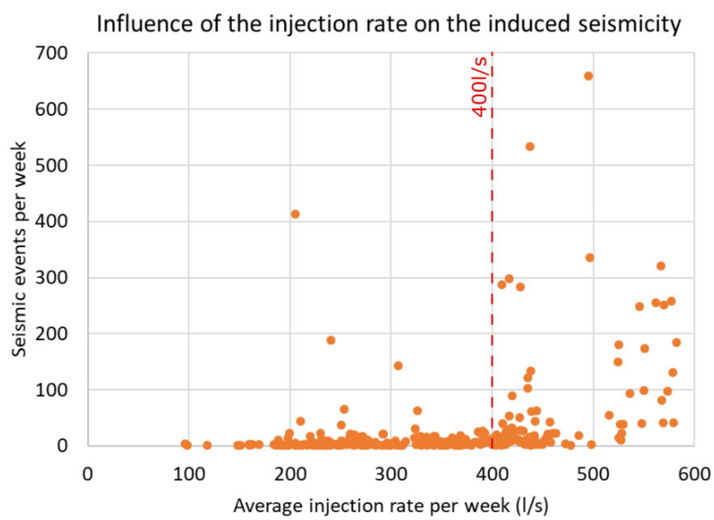

Figure 23: Influence of the injection rate on the induced seismicity from September 2011 to June 2018 (Seismic catalog SIL Network)

However, when we focus on the daily evolution of the seismicity and the influence of the injection rate on the induced seismicity is less clear (Appendix 18 and Appendix 19). The immediate response of the seismicity in September 2011 is clear but the two intense seismic periods in mid-2013 to early-2014 and mid-2016 to mid-2017 visible on the Figure 22 did not seem to be correlated to a change of the injection rate.

The Figure 24 shows the number of seismic events per day (seismic catalog : Kristjánsdóttir, 2018) and the injection rate for active wells in the Húsmúli area from September 2011 to May 2012. During this period, the correlation between injection rate and the intensity of the seismicity is poorly visible. From September to end of October there is not a day-to-day correlation between injection rate and induced seismicity. Seismic events occurred almost every day and the offset of the seismic response varies from 1 to 5 days according to the impacting well, the distance and the orientation of the active fault. In the following period, seismicity occurred less often but a correlation stays not visible. For example, seismic peaks occurred in mid-December, mid-January and early March do not seem to be linked to a change of the injection rate.

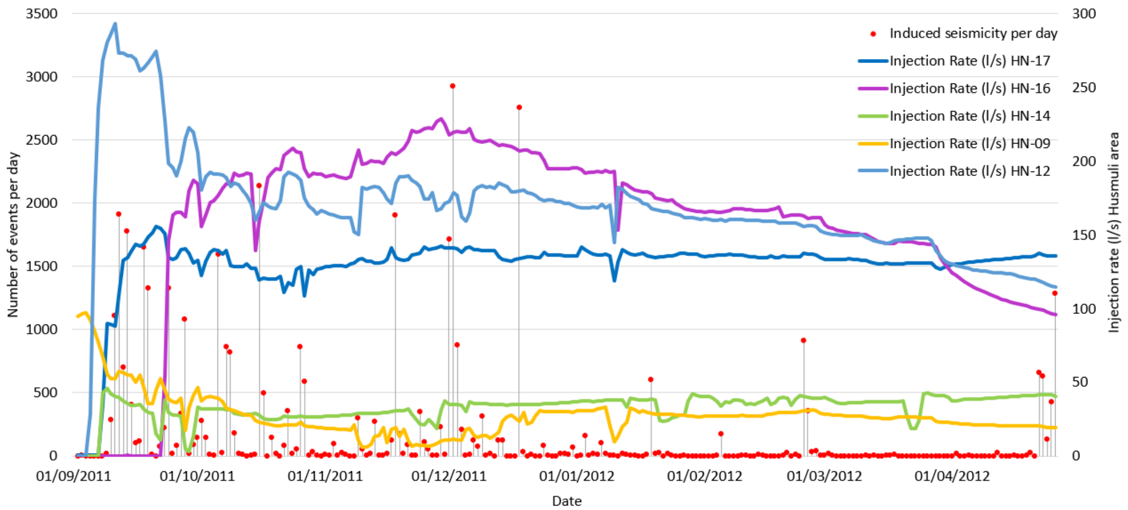

Figure 24: Evolution of the injection rate and the induced seismicity from the onset of the injection (September 2011) to May 2012 (Seismic catalog: Kristjánsdóttir, 2018).

Spatial distribution of the seismicity in function of the injection point

The spatio-temporal evolution of the seismicity is used to understand the evolution of the reservoir state along the injection. The Figure 25 shows the evolution of the distance of the seismicity from the clusters of the three more active in the Húsmúli area during the 250 first days of the injection. The cluster of wells HN-12, HN-16 and HN-17 represents more than 80% of the total injection in the Húsmúli area.

During the first 100 days of the injection the increase of the distance of the seismicity from the well cluster is clearly visible (from 2500 to 3500 m away). Then, this distance starts to decrease correlated to a drop of the seismicity (in term of number days with seismic events and of number of events per day) and the decrease of the injection rate until day 170. Towards the end of the analyzed period (170 days), the events closer to the wells cluster (5% closest hypocenters) are, in average, further away (750 m) than at the beginning (100 m).

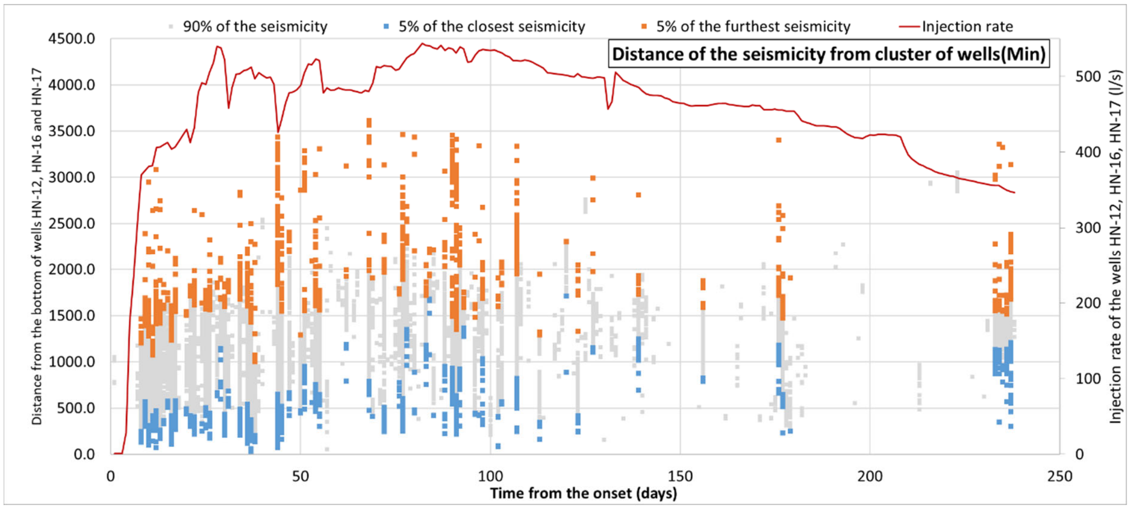

Figure 25: Evolution of the distance of the seismicity from the cluster of wells HN-12, HN-16, HN-17 based on the closest distance from each well and total injection rate of the well cluster (HN-12, HN-16, HN-17) (Seismic catalog: Kristjánsdóttir, 2018).

The first 100 days seem to represent the propagation of the injection and reservoir change in Húsmúli area. After this period, there is not events occurred farer from the well cluster which means the reaching of the boundary of the affected area in Húsmúli. The decrease of the distance of the seismicity may be correlated to the decrease of the injection rate or to the return to an equilibrium in the reservoir.

Conclusion

It is clearly visible that the injection highly impacted the Húsmúli area and triggered a series of seismic swarms immediately after the onset of the injection and during all the period of the injection. The injection rate seems to play a role on the generation of the seismicity. When the injection rate reaches more than 400 l/s the risk of seismicity tends to be higher with an increase of the event frequency.

However, the daily variation of the injection rate was not linked with the evolution of the seismicity. Indeed, this absence of correlation is likely due to the complexity of the fault network and the multi-wells injection evolution. The requirements for the activation of a fault are not only based on the injection rate but also based on the distance of the fault from the injection source, the orientation of the faults and the connection between the fault and the injection sources.

The influence of the injection rate on the generation of induced seismicity is undeniable and trends along years of injection are clearly visible. The spatio-temporal evolution of the seismicity allows an understanding of the propagation of changes in the reservoir in term of spatial distribution and in term of frequency of seismic swarms.

To have a better understanding of the evolution of these changes in the reservoir it is necessary to study the pressure evolution of the reservoir in time.

5.4.2. Estimation of the pressure impact in the Húsmúli area

The flow rate has an impact on the generation of the seismicity but, the reactivation of faults is the consequence of a pressure or a stress field change. Therefore, the study of the pressure evolution in the reservoir is important to understand the evolution of the seismicity. However, the bottom well pressure is not available for injected wells in Húsmúli. The analysis of the link between the spatio-temporal evolution of the pressure in the reservoir and the activation of seismic events is based on the simulation pressure model (ISOR). This pressure model is calculated with TOUGH2 based on the resolution of equilibrium energy equations (including fluid flow and thermal flows, based on a type of Darcy advection extended to multiphases and a diffusive transport).

We calculated the pressure evolution along a well to estimate the uncertainty of the model and the theorical consequence of the injection on the reservoir state. To estimate the initial pressure in the well we took into account the water table (≈280 m for the well HN-12) and the temperature of the reservoir. The HN-12 bottom well temperature is ≈250 °C at 1476 m depth TVD. We average temperature in the along the HN-12 to estimate the water density which is an important factor to calculate the pressure. The blue line in the Figure 26 represents the initial pressure in the well HN-12 before injection (Figure 26).

The grey line represents the well pressure during the injection when only the pumping pressure (8 bars) and the shift in the water table are taken into account. Values extracted from the TOUGH2 model show a progressive increase of pressure in time. After 3 months of injection pressure had increased by 2 MPa at 1500 m depth which corresponds to an increase of 15% of the initial pressure.

The theorical estimations show a maximum increase of 3.2 MPa from the onset of injection. Therefore, the increase pressure in the reservoir should not exceed 3.2 MPa.

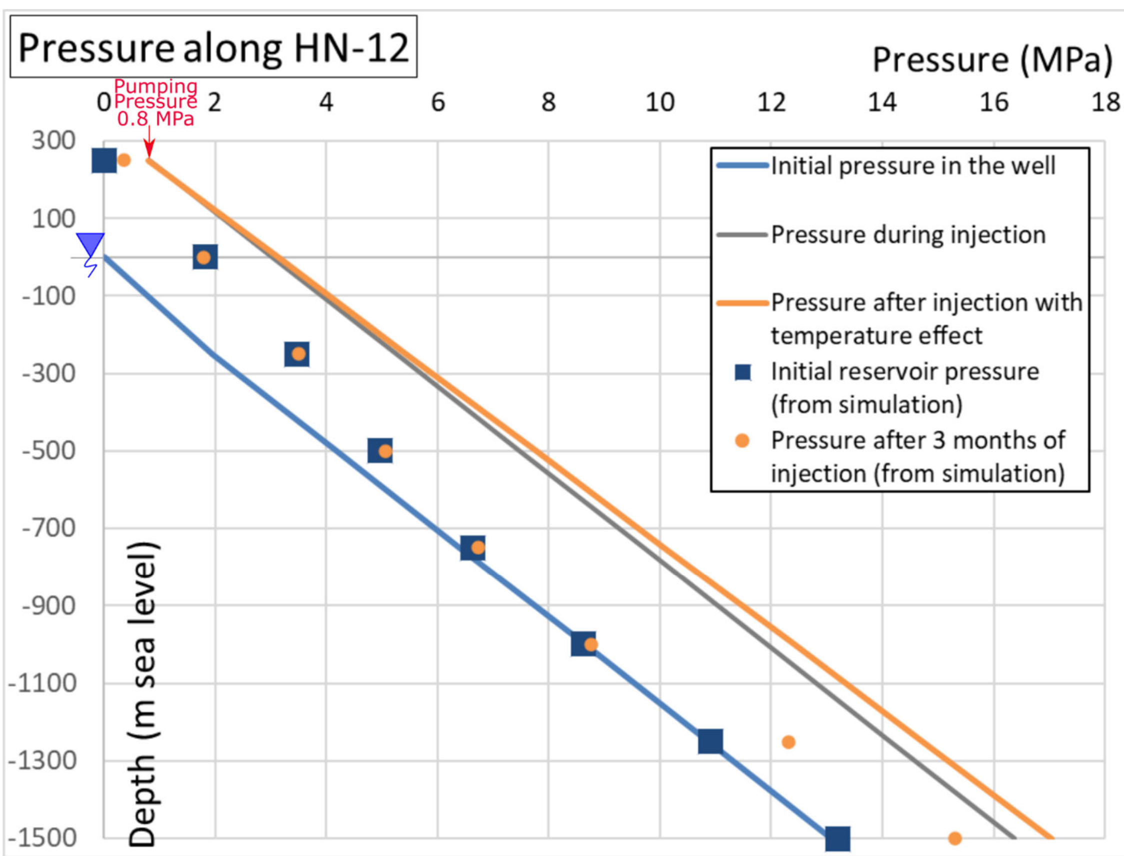

Figure 26: Evolution of the pressure in the well HN-12 before and during the injection. Analytic results (representing by lines) and simulation results (representing by dots) from hydraulic model TOUGH2 (ISOR).

Based on the pressure evolution from the Tough 2 model, we correlated local pressure change with the activation of faults depending on their orientation. The pressure model in the TOUGH2 model

(ISOR) represents a grid of points from the surface to 2.3 km depth, eight pressure points located on activated faults were selected at 1.9 km depth. Faults selected shows a representative sample of fault orientations in the Húsmúli area (N0°, N10°, N30°, N50°, N60°). Analysis behind the Figure 27 and Figure 28 are based on the simulation pressure model from the TOUGH2 Model (ISOR).

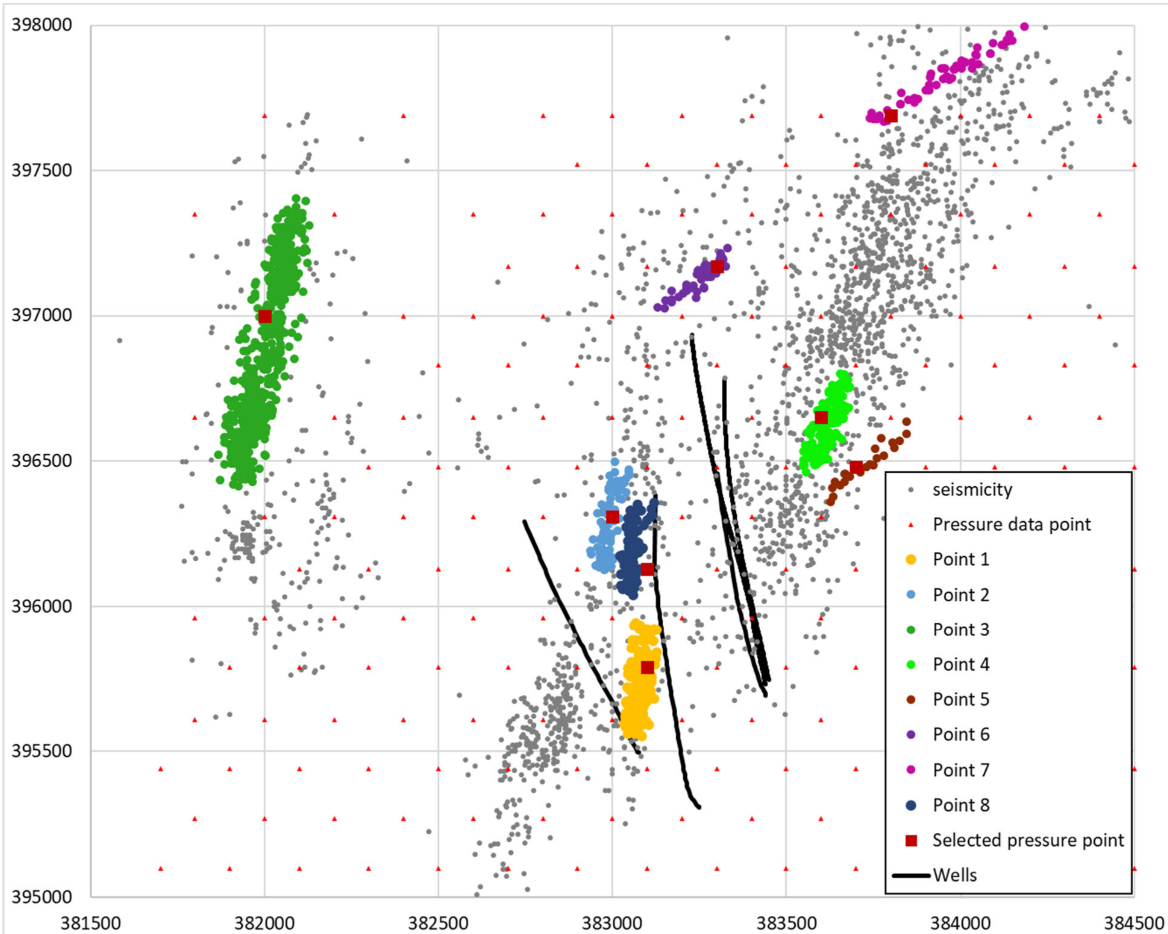

Figure 27: Map of the seismicity from 1.8km to 2km depth highlighting faults activated during the injection (September 2011- May 2012) and pressure data point selected (Seismic catalog: Kristjánsdóttir, 2018, Pressure data : Tough 2 model, ISOR).

Despite the large spatial distribution of selected faults in the Húsmúli area, the seismicity occurred quickly after the beginning of the injection, the seismic response occurred between 5 days (Points 4), for structures close to injection points to 43 days (Points 3) for the furthest structures (Figure 24).

At 1.9 km depth, the pressure evolution from September 2011 to May 2012 exceeds an increase of 3.2 MPa. The selected point 2 and 8 represent the most pressure increase (≈3.8 MPa) due to their close location from injection points. Therefore, the increase of the pressure at the bottom hole is higher than 3.2 MPa and must be explained by another factor of pressure increase and not only by the pump pressure and the water table.

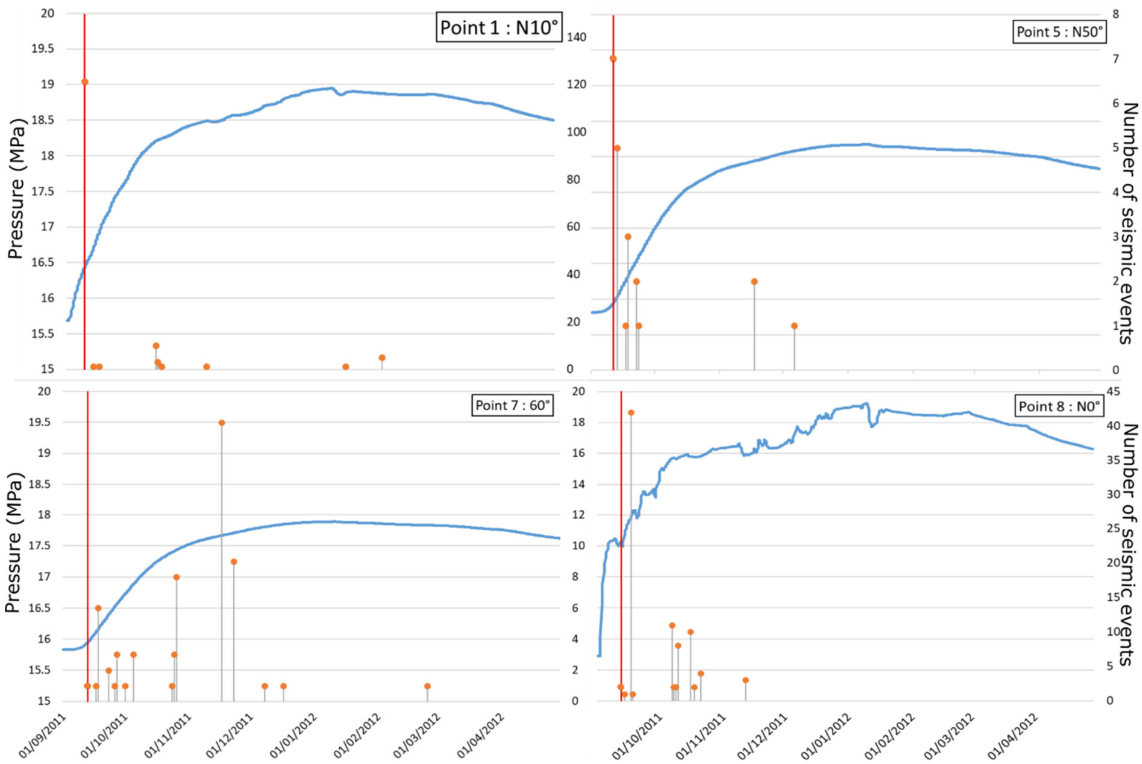

Figure 28: Pressure evolution at 1.9 km depth of the selected point 1, 5, 7 and 8 and number of seismic events per day located along selected faults (Seismic catalog: Kristjánsdóttir, 2018, Pressure data : TOUGH 2 model, ISOR). The red line represents the first seismic activity along the selected fault.

The pressure delta between the initial pressure and the pressure of the first seismic events is between 0 to 2.09MPa for the same depth. The activation of specific orientations (N0°, N10°, N30°, N50°, N60°) is in correlation with the position of these orientations in the Mohr circle and the range of pressure delta needed for the activation shows how instable are these orientation faults in the Húsmúli area (part **Error! Reference source not found.**).

5.4.3. Temperature of the injected fluid

The temperature of the injected fluid influences the injection rate and the pressure in the reservoir. Gunnarsson (2013) describes the link between the temperature of the injected fluid and the injectivity (Appendix 19). Observations highlights a significant increase of the injection rate when the temperature of the injected fluid is low. Gunnarsson (2013) explained this dependency by fracture dominated permeability. The thermal expansion/contraction is an effect controlling aperture changes of fractures.

Moreover, the injection of cold water also seems to induce more seismicity than hot water (Gunnarsson, 2013). The cooling generated by the injection of cold water can induce thermal stresses and may cause a shear failure in existing faults and factures around the well. Observation in the Geyser field (USA) highlights this phenomenon (Jeanne et al., 2014; De Simone et al., 2017). Moreover, the cooling of the area around the well make the water denser. The density change of the water plays a role in the long-term increase of pressure during injection.

Unfortunately, the temperature evolution of the injected fluid is not available for wells in the Húsmúli area. According to Gunnarsson (2013), the temperature varies from around 70 °C to 105 °C. These temperatures are lower than the reservoir temperature at injection depth (≈250 °C at 1.5 km depth) and will generate a change of water density along the well. The orange line (Figure 26) takes into account the density changes in function of depth. At 1500 m depth the pressure delta between the initial pressure and the and the orange line, considering a decrease of 40 °C of the average temperature around the well (i.e. 160 °C to 120 °C), is about 4 MPa, 0.8MPa more than the grey line. This effect explains the pressure increase of 3.8 MPa of the point 2 and 8 and may be one reason explaining the temperature depend of the injection rate. This increase of pressure around the well will progressively change the pressure of the reservoir.

5.4.4. Impacts of the injection on the Húsmúli area.

The pressure evolution guides the activation of faults which are really sensible to changes in the Húsmúli area. However, the pressure evolution can be guided by other factors. The injection rate and the temperature of the injected fluid described above influence the pressure evolution and thus, the induced seismicity are dependent of these factors.

An important flow rate (more than 400 l/s) and/or a low temperature of injected fluid accentuate the pressure change through an increase of the pressure or through a quicker propagation of the affected zone. A monitoring of the injected fluid temperature, the bottom hole pressure and the flow rate is necessary to manage the induced seismicity.

6. Hydro-geomechanical framework (ETH)

The modelling activities in the COSEISMIQ project have two main focuses: 1) understanding the physical processes leading to induced seismicity by accounting the specific conditions of the Hengill region (GES); 2) implementing the hydro-geomechanical framework for applications in real-time for Iceland (ETH).

For the hydrological modelling, a regional TOUGH2 model covering the Hengill area is used based on previous work by Reykjavik Energy and partners (Bjornsson et al. 2003; Gunnarsson et al., 2011; Aradóttir et al., 2012; Tómasdóttir, 2018; Ritz et al., 2020). The choice of a TOUGH-based model allows to account for multiphase flow, which, given the flow conditions in Hengill area (liquid water, steam, and perhaps supercritical water), is critical to achieving realistic results. We employ a hybrid approach by combining TOUGH-base models with a stochastic approach to simulate induced seismicity (e.g. Rinaldi & Nespoli, 2017). As to the geomechanical part of the hybrid modelling, two different approaches are chosen for the different focuses of the project. For the first objective, we use the ETH-developed "seed-model" in 3D to test physical processes in addition to pore pressure propagation; for the second objective and to have a robust and performant forecasting model, we use an analytical version to understand the potential for induced seismicity.

6.1. TOUGH2 Hengill Regional Model

The large scale TOUGH2 model for the Hengill geothermal field was provided by Reykjavik Energy. The model for Hengill covers an area of 50 km by 50 km with a depth of 3000 m. It comprises nearly 43.000 elements categorised into 43 reservoir domains. The mesh is centred around the production areas West of Húsmúli, with a refinement of the grid in the centre. 129 production and 31 injection time series cover multiple decades of hydraulic data (source/sinks since the 1970s, production since the 1990s). Figure 29 shows the state of pressure in the regional model before the start of the reinjection in Húsmúli. The centre of the mesh with depleted pressures corresponds to the production area that has been active prior to the reinjection. The Húsmúli reinjection zone is located at the edge of the depleted area (see red highlight in Figure 29).

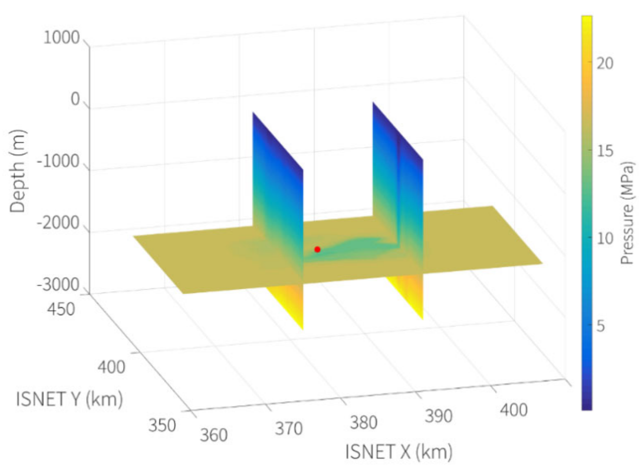

Figure 29: Initial pressure in the Hengill area before the start of reinjection in Húsmúli (September 2011) computed with TOUGH2 on the regional model accounting for the production and hydraulic data since the 1970s.

In this deliverable, we focus on the Húsmúli reinjection area between September 2011 and May 2012. Five wells are actively injecting in Húsmúli during the period of interest, their representation in the TOUGH model is summarised in Table 3: Injection wells active in the TOUGH model for Húsmúli The injection rates (Figure 30) show a dominance of well HN12 at the beginning of the reinjection, Then picked up by wells HN16 and HN17. The deepest well, HN09, is relatively quiet due to its penetrating the consolidated basaltic layer and thus having low injectivity.

Table 3: Injection wells active in the TOUGH model for Húsmúli

Well	Coordinates injection (Tough model)		
	ISNET X	ISNET Y	Depth (m)
HN09	3.831E+05	3.96134E+05	1900
HN12	3.833E+05	3.96480E+05	1550
HN14	3.828E+05	3.96307E+05	1550
HN16	3.834E+05	3.96654E+05	1550
HN17	3.833E+05	3.96480E+05	1550

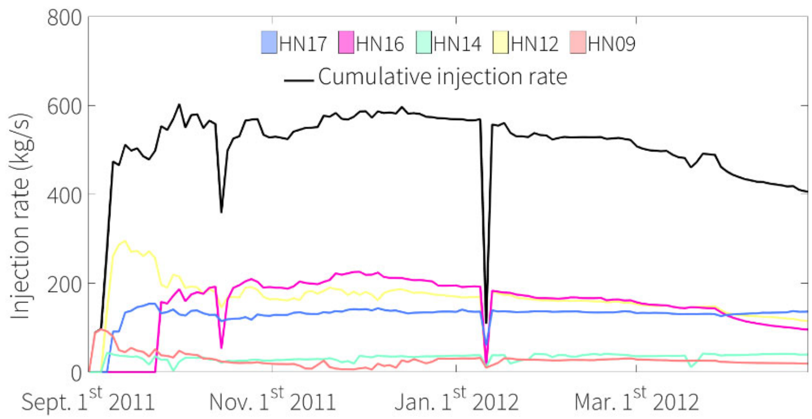

Figure 30: Injection rate for the individual wells and cumulative rate of the Húsmúli reinjection zone

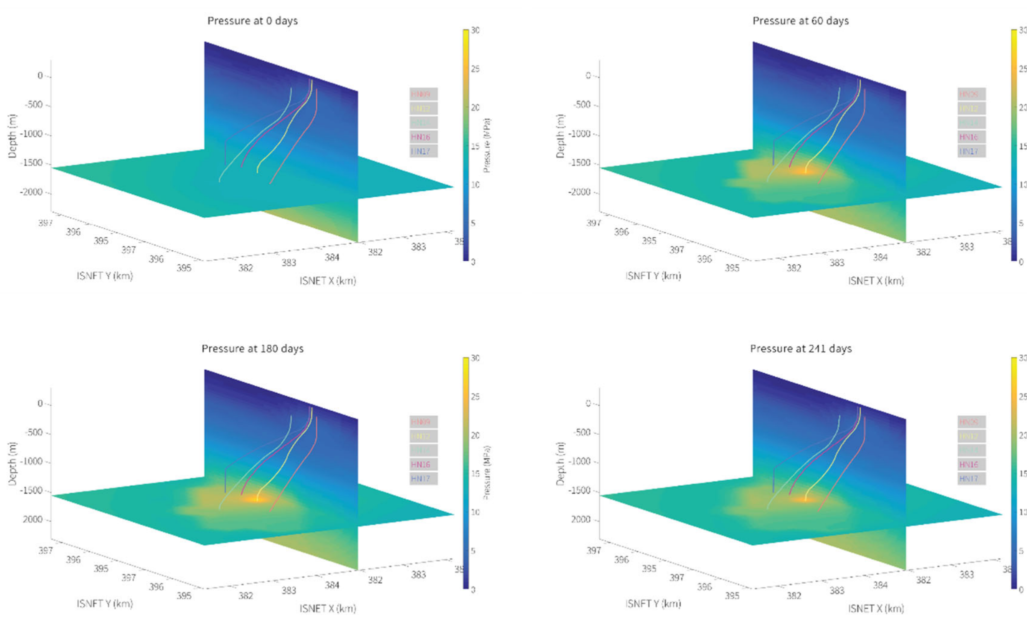

Figure 31: Evolution of the pressure in Húsmúli from the start of reinjection into wells HN9 to HN17

The calculated pressure solution for Húsmúli is shown in Figure 31 (representative selection of time steps). The main feature shows that the high injection rates in well HN12 clearly dominate the pressure distribution in the system at early time steps. The other wells do partially pick up after the initial onset of pressure increase, but overall, the pressure signal is dominated by well HN12. The calculated pressure closely follows the injection rates for the individual wells, with HN12 clearly having a much larger rate at early stages (Figure 2)

6.2. 3D-Seed Model

TOUGH2-seed is a hybrid simulator, combining TOUGH2 for the multi-phase and multi-component fluid flow calculation with a stochastic geomechanical model (Rinaldi & Nespoli, 2017). The seed model creates a random distribution of weaknesses (potential earthquake hypocentres) that can be reactivated if necessary pressure/stress conditions are reached. This geomechanical model accounts for a complete 3D stress field with input such as the regional stress regime, the orientation of the stress field and allows heterogeneities (major faults, zones of higher seed density) with specific orientation (dip and strike) provided by the structural analysis performed as part of this Work Package. At each time step, the pore pressure calculated by TOUGH2 is interpolated at each seed location, and the principal stresses are then updated to account for pore pressure changes. Once the principal stresses are reassigned, the shear and normal stresses τ and σ_n are computed at each seed which are then checked for reactivation using a Coulomb failure criterion. If reactivation of a given seed, a magnitude is randomly selected within a Gutenberg-Richter distribution depending on the b-value (Schorlemmer et al. 2005, Goertz-Allmann & Wiemer 2013). After reactivation, the seeds' shear stress state is modified with stress drop.

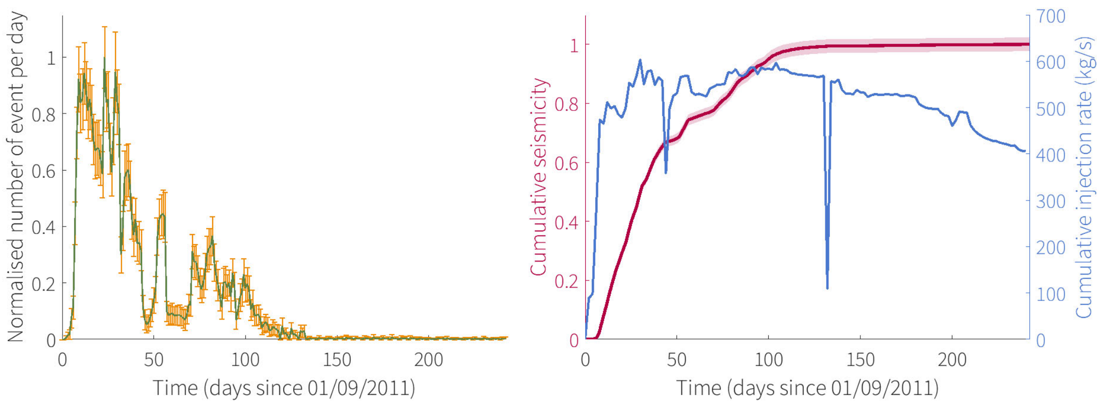

Figure 32: Seismicity rates (left) and cumulative seismicity with standard deviation (right) modelled with the 3D Seed model

We run 100 single realizations with the same pressure solution and average the results on the set of realizations, by stochastically varying the seeds position, orientation, friction coefficient, and local stress conditions. The cumulative number of induced events and seismicity rates are shown inFigure 32. Seismicity increases with the onset of injection, marking a slight delay from the start of injection to the first simulated events. The rates then decrease as the injection rate stabilises and decreases. The decrease of seismicity after the initial outburst seem to match reported decreases in the number of recorded events with the stabilisation and decrease of the injection rate in late 2011 and 2012 (Gunnarsson, 2013; Flóvenz et al., 2015). However, recorded data show that even if the seismicity rate decreases, events keep happening in temporal clusters for example around day 175 (ca. March 1st 2012) and the last days of April 2012 around day number 235 (Figure 33).

Figure 1

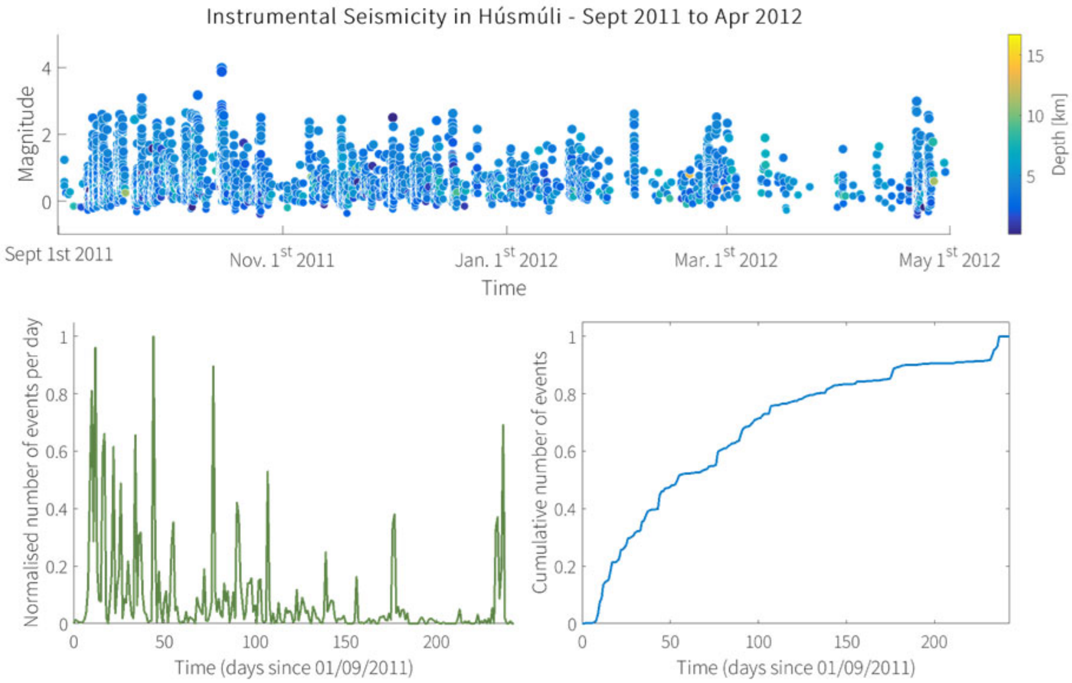

Figure 33: Instrumental seismicity in Húsmúli (SIL network) recorded during the period modelled

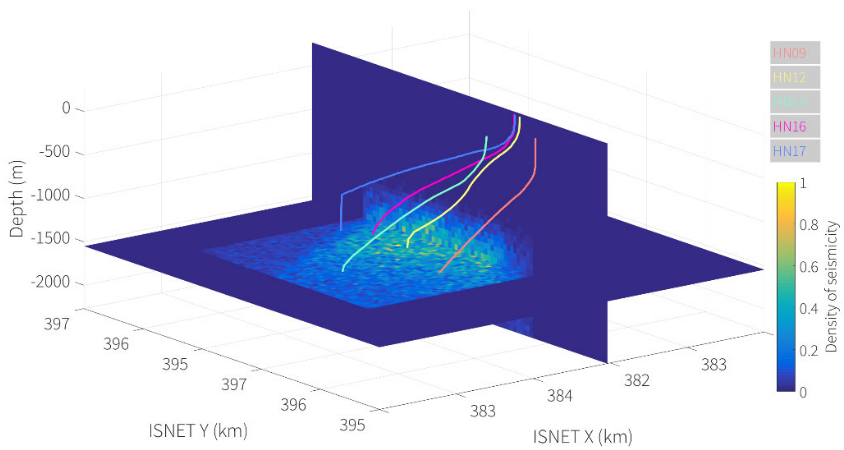

Figure 34: Density of seismicity modelled with the 3D Seed model (averaging over the 100 stochastic realisations)

The concatenation of the stochastic realization (**Error! Reference source not found.**) shows the direct effect of pressure increase on the seismicity density, with the central area around well HN12 dominating the modelled seismic signal. In future modelling work, the full coupling of TOUGH2-Seed will allow us to account for secondary mechanisms of triggering such as static stress transfer as well as coupling the permeability changes to the TOUGH2 pressure solution. These further steps could show a different spatial and temporal pattern of seismicity, potentially favoring an extended sequence both in space and time.

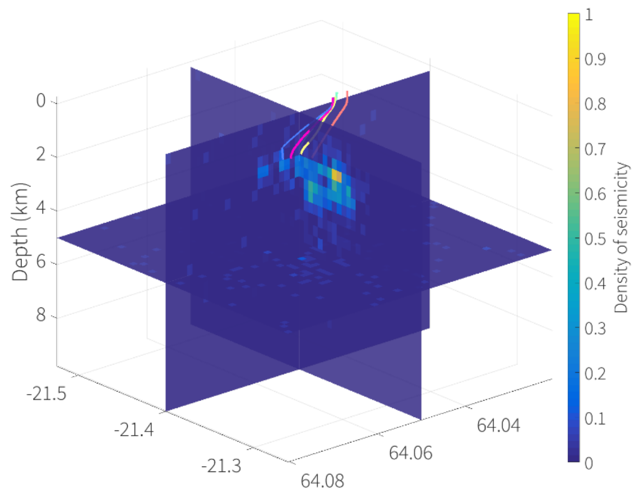

Figure 35: Instrumental seismicity in Húsmúli (SIL network) in 3D recorded between September 2011 and April 2012. Note the depth range larger than the modelled seismicity in Error! Reference source not found.**.**

6.3. Analytical Seed Model

The analytical version of the Seed model has been derived so that it can be coupled with any flow model exporting the simulated pressure evolution. This analytical model is here coupled to the TOUGH2 model of the Hengill area.

This analytical model considers two-dimensional Mohr-Coulomb circles for the seeds, with two principal stresses $\sigma_3 < \sigma_1$ changing with depth and following normal distributions. Then, the analytical Cumulative Density Function (CDF) and Probability Density Function (PDF) of a hypocenter being reactivated at a certain pressure P_f is found for the hydrostatic conditions of each depth. These analytical solutions are truncated to the lowest positive value P_f for which reactivation of fractures is expected and a numerical integration with depth may be needed. Besides the principal stresses, the solutions are conditioned on the orientation of the fracture and to the frictional properties of the fracture (i.e. friction and cohesion).

Especially for simulations, where the hydraulic effect of the seeds is not modelled, such analytical equations make Monte Carlo integrations obsolete. The converged solution can be returned very quickly for the simulated evolution of the overpressure, simply by tracking the evolution of the maximum pressure experienced inside the reservoir. The final forecast from the analytical model is normalized to the density with which potential hypocenters are expected to be distributed inside the reservoir. The analytical model will be extended in returning the analytical predictions of the b-value for seismicity, in scenarios where the b-value and the differential stress $\Delta\sigma=(\sigma_1-\sigma_3)$ are correlated.

The analytical model we present accounts for the distribution of strikes in the structures in Húsmúli as a probability density function of orientation for the rupture points. The spatial extent of the modelled seismicity shows similar patterns as the 3D-Seed model (Figure 36 and Figure 37), The spatial seismicity signal is again dominated by well HN12 due to its high injection rates at the onset of reinjection.

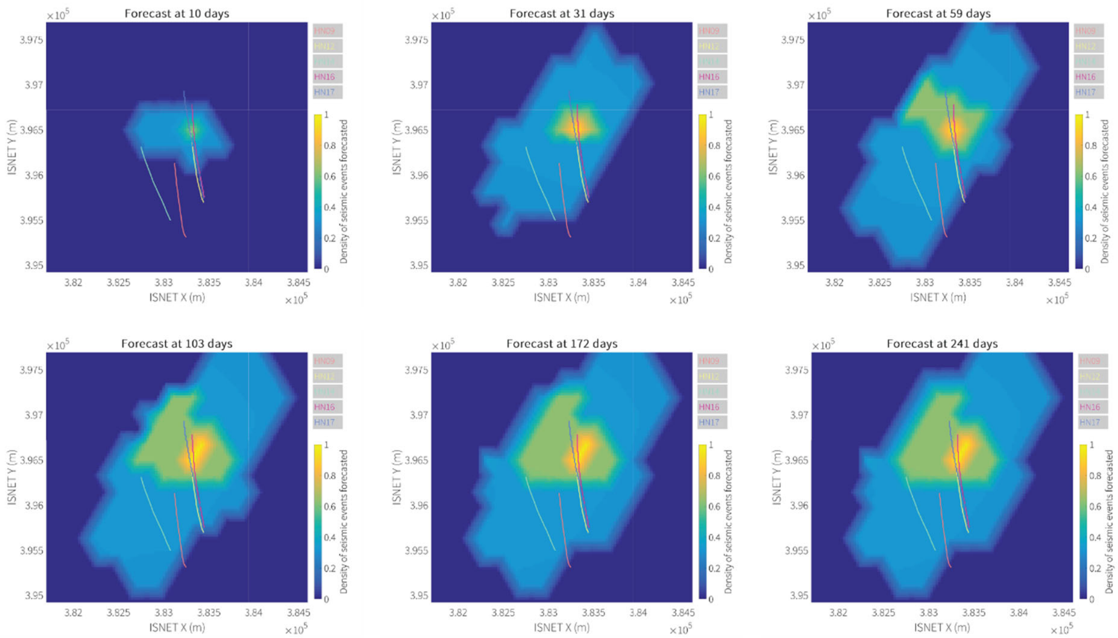

Figure 36: Map view of the evolution of the density of seismic events at depth 1550 m

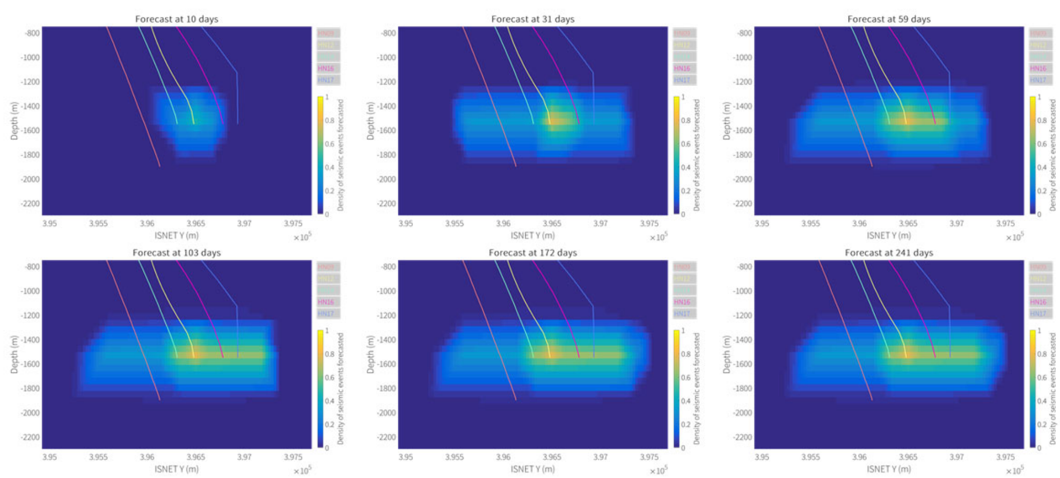

Figure 37: Vertical slice of the evolution of the density of seismic events

The analytical Seed model provides very similar results to the 3D Seed model in terms of the temporal evolution of seismicity (Figure 38). Seismicity increases with the onset of injection, marking a slight delay from the start of injection to the first simulated events. The rates then decrease as the injection rate stabilizes and decreases. Compared to the recorded seismicity, the simulated set follows a smoother path, closely related to the increase of the maximum pressure (Figure 38).

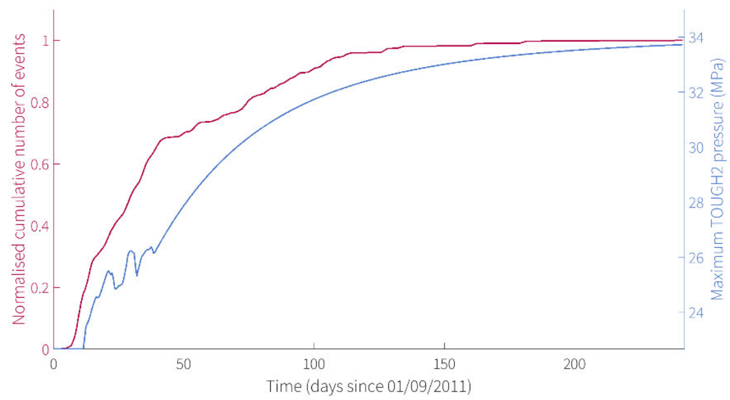

Figure 38: Cumulative seismicity modelled with the analytical Seed model compared to the recorded seismicity in the SIL catalogue and the maximum pressure in time in the TOUGH2 model

7. Conclusion

The aim of this work is to analyse the factors playing a role in the occurrence of induced seismicity associated to water injection. Our results show the implication of several parameters on the generation of induced seismicity.

The structure and tectonic background of the region exert an important influence on the induced seismicity. In Húsmúli, natural seismicity occurred before the onset of injection (e.g. during the seismic episode of 1990's), which implies a natural tectonic loading of the structures that are present in the area. The presence of unstable faults makes the area very favorable to generate induced seismicity. According to the stress assessment, most structural orientations are very near or at the threshold of reactivation.This conclusion is reinforced by the observation that seismicity was triggered very early in the injection history associated to relatively small increases of fluid pressures (<3 MPa).

The seemingly patchy reactivation pattern of seismic events in time cannot be explained by the application of a homogenous stress state (i.e a stress state constant in time and applicable to the whole area), since all faults seem to be at the brink of reactivation when such a stress is applied. Observed patterns of fault reactivation might indicate dynamic changes during the injection. Modifications of the local stresses associated to stress transfer seem so far, the most likely explanation for this, but other processes like an anisotropic pressure field or dynamic triggering have not been ruled out.

The temperature also influences the friction and can define the slip behavior during deformation. Above 550 °C±150 °C, the slip along faults should be mostly aseismic (semi-brittle field) and thus the number of localized events should be very scarce. Above around 300°C (e.g. below 2.2/3.4 km depth), the parameter a-b, that describes the slip behavior, tends to decrease and thus, seismic slip tends to be less frequent. Moreover, if the bottom limit of the seismogenic layer described as the upper limit of the semi-brittle field represents the 90% of the number of seismic events from the surface, this limit should be at around 2.8 km depth in the Húsmúli. However, regarding the geothermal gradient in the Húsmúli area, the potential temperature at 2.8 km does not exceed 300/320 °C and might not reflect the base of the seismogenic layer but, may correspond to the beginning of a frictional change in the reservoir (at ≈300°C).

The hydraulic management is another important factor influencing pressure changes in the reservoir and thus, the seismic risk. Injection flow rates above a threshold of 400l/s seem to trigger a significantly higher number of seismic events.

With the implementation of these parameters the hydro-mechanical model tends to make more realistic processes, which occurred in the Húsmúli area. Both models presented here are able to produce seismic catalogues from the pressure solution calibrated for the Hengill area. The models illuminate similar areas mostly concentrated around the shallower wells, and in particular HN-12, which dominates the pressure signal and thus logically dominates the seismic signal because of the intrinsic relation between (maximum/pore) pressure and reactivation in the Mohr-Coulomb failure criterion. The temporal evolution of the modelled seismicity is shown in Figure 33 for both models. The simulated seismicity accumulates faster than the observed seismicity due to the very quick increase of pressure in the reservoir in the early period simulated. Both models tested here rely only on a direct relationship between pressure and failure, the discrepancy between the modelled and observed seismicity can be explained by the absence of secondary mechanisms such as static stress transfer, porosity enhancements etc.

Further steps of the modelling will include thermal and rheological components to account for more complex physical processes at play in a volcanic system such as Hengill. The 3D-Seed model will also be run on a fully coupled version to see the effects of permeability changes, earthquake interaction and more complex stress modifications. The addition of such secondary mechanisms should yield models able to better fit the observed seismicity rates.

References

Adelinet, M., Fortin, J., Schubnel, A., & Guéguen, Y. (2013). Deformation modes in an Icelandic basalt: from brittle failure to localized deformation bands. *Journal of volcanology and geothermal research*, *255*, 15-25.

Aradóttir, E. S. P., Sonnenthal, E. L., Björnsson, G., & Jónsson, H. (2012). Multidimensional reactive transport modeling of CO2 mineral sequestration in basalts at the Hellisheidi geothermal field, Iceland. International Journal of Greenhouse Gas Control, 9, 24-40.

Arnason, K., & Magnusson, I. Þ. (2001). Geothermal activity in the Hengill area. Results from resistivity mapping. Orkustofnun report, in Icelandic with English abstract, OS, 91, 2000.

Batir, J., Davatzes, N. C., & Asmundsson, R. (2012). Preliminary model of fracture and stress state in the Hellisheidi Geothermal Field, Hengill Volcanic System, Iceland. In Proceedings of the Thirty-Seventh Workshop on Geothermal Reservoir Engineering, Stanford.

Bao, X., & Eaton, D. W. (2016). Fault activation by hydraulic fracturing in western Canada. Science, 354(6318), 1406-1409.

Bessason, B., Sólnes, J., Bjarnason, J. Ö., Guðmundsson, A., & Steedman, S. (2012). Comprehensive damage analysis of buildings affected by the 2008 South Iceland earthquake. In *Proceedings of the 15th World Conference of Earthquake Engineering*.

Bjornsson, G., Hjartarson, A., Bodvarsson, G. S., & Steingrimsson, B. (2003, May). Development of a 3-D geothermal reservoir model for the greater Hengill volcano in SW-Iceland. In Proceedings: TOUGH Symposium (pp. 1-11).

Blanpied, M. L., Lockner, D. A., & Byerlee, J. D. (1995). Frictional slip of granite at hydrothermal conditions. Journal of Geophysical Research: Solid Earth, 100(B7), 13045-13064.

Bommer, J. J., Oates, S., Cepeda, J. M., Lindholm, C., Bird, J., Torres, R., ... & Rivas, J. (2006). Control of hazard due to seismicity induced by a hot fractured rock geothermal project. *Engineering Geology*, *83*(4), 287-306.

Broccardo, M., Mignan, A., Grigoli, F., Karvounis, D., Rinaldi, R. P., Danciu, L., ... & Hjörleifsdóttir, V. (2019). Induced seismicity risk analysis of the hydraulic stimulation of a geothermal well on Geldinganes, Iceland. *Natural Hazards and Earth System Sciences Discussions*.

Clifton, A. E., Sigmundsson, F., Feigl, K. L., Guðmundsson, G., & Árnadóttir, T. (2002). Surface effects of faulting and deformation resulting from magma accumulation at the Hengill triple junction, SW Iceland, 1994–1998. *Journal of volcanology and geothermal research*, *115*(1-2), 233-255.

Cornet, F. H., Helm, J., Poitrenaud, H., & Etchecopar, A. (1997). Seismic and aseismic slips induced by large-scale fluid injections. In Seismicity associated with mines, reservoirs and fluid injections (pp. 563-583). Birkhäuser, Basel.

De Simone, S., Carrera, J., & Vilarrasa, V. (2017). Superposition approach to understand triggering mechanisms of post-injection induced seismicity. *Geothermics*, *70*, 85-97.

Duboeuf, L. (2018). Injections de fluide dans une zone de faille (LSBB, Rustrel): sismicité induite et déformation asismique(Doctoral dissertation, Côte d'Azur).

Ellsworth, W. L. (2013). Injection-induced earthquakes. Science, 341(6142), 1225942.

Flóvenz, O. G., Ágústsson, K., Guðnason, E. Á., & Kristjánsdóttir, S. (2015, April). Reinjection and induced seismicity in geothermal fields in Iceland. In Proceedings of world geothermal congress.

Franzson, H., Kristjánsson, B. R., Gunnarsson, G., Björnsson, G., Hjartarson, A., Steingrímsson, B., ... & Gíslason, G. (2005). The Hengill-Hellisheiði geothermal field. Development of a conceptual geothermal model. In Proceedings world geothermal congress (pp. 1-7). Antalya.

Fridleifsson, G. O., & Elders, W. A. (2005). The Iceland Deep Drilling Project: a search for deep unconventional geothermal resources. *Geothermics*, *34*(3), 269-285.

Foulger, G. R. (1988). Hengill triple junction, SW Iceland 2. Anomalous earthquake focal mechanisms and implications for process within the geothermal reservoir and at accretionary plate boundaries. *Journal of Geophysical Research: Solid Earth*, *93*(B11), 13507-13523.

Gischig, V. S., & Wiemer, S. (2013). A stochastic model for induced seismicity based on non-linear pressure diffusion and irreversible permeability enhancement. *Geophysical Journal International*, *194*(2), 1229-1249.

Goertz-Allmann, B. P., & Wiemer, S. (2013). Geomechanical modeling of induced seismicity source parameters and implications for seismic hazard assessment. *Geophysics*, *78*(1), KS25-KS39.

Grigoli, F., Cesca, S., Priolo, E., Rinaldi, A. P., Clinton, J. F., Stabile, T. A., ... & Dahm, T. (2017). Current challenges in monitoring, discrimination, and management of induced seismicity related to underground industrial activities: A European perspective. *Reviews of Geophysics*, *55*(2), 310-340.

Gunnarsson, G., Arnaldsson, A., & Oddsdóttir, A. L. (2011). Model simulations of the Hengill area, Southwestern Iceland. Transport in porous media, 90(1), 3-22.

Gunnarsson, G. (2013). Temperature Dependent Injectivity and Induced Seismicity–Managing Reinjection in the Hellisheiði Field, SW-Iceland. GRC Transactions, 37, 1020-1025.

Gunnarsson, G., Kristjánsson, B. R., Gunnarsson, I., & Júlíusson, B. M. (2015). Reinjection into a fractured reservoir—induced seismicity and other challenges in operating reinjection wells in the Hellisheiði Field, SW-Iceland. In Proceedings world geothermal congress.

den Hartog, S. A., Peach, C. J., de Winter, D. M., Spiers, C. J., & Shimamoto, T. (2012). Frictional properties of megathrust fault gouges at low sliding velocities: New data on effects of normal stress and temperature. *Journal of Structural Geology*, *38*, 156-171.

He, C., Wang, Z., & Yao, W. (2007). Frictional sliding of gabbro gouge under hydrothermal conditions. Tectonophysics, 445(3-4), 353-362.

Healy, J. H., Rubey, W. W., Griggs, D. T., & Raleigh, C. B. (1968). The denver earthquakes. Science, 161(3848), 1301-1310.

Hensch, M., Lund, L., Brandsdóttir, B., (2016), Temporal stress changes associated with the 2008 May 29 MW 6 earthquake doublet in the western South Iceland Seismic Zone, Geophys. J. Int. 204, 544–554.

Hjörleifsdóttir et al., (2019). Induced earthquakes in the Hellisheiði geothermal field, Iceland. 3rd Schatzalp Workshop on Induced Seismicity.

Jeanne, P., Rutqvist, J., Vasco, D., Garcia, J., Dobson, P. F., Walters, M., ... & Borgia, A. (2014). A 3D hydrogeological and geomechanical model of an Enhanced Geothermal System at The Geysers, California. *Geothermics*, *51*, 240-252.

Kao, H., Eaton, D. W., Atkinson, G. M., Maxwell, S., & Mahani, A. B. (2016). Technical meeting on the traffic light protocols (TLP) for induced seismicity: summary and recommendations. *Geological Survey of Canada, Open File*, *8075*.

Karvounis, D. C., Gischig, V. S., & Wiemer, S. (2014). Towards a real-time forecast of induced seismicity for enhanced geothermal systems. In *Shale Energy Engineering 2014: Technical Challenges, Environmental Issues, and Public Policy* (pp. 246-255).

Keiding, M., Lund, B., & Árnadóttir, T. (2009). Earthquakes, stress, and strain along an obliquely divergent plate boundary: Reykjanes Peninsula, southwest Iceland. *Journal of Geophysical Research: Solid Earth*, *114*(B9).

Khodayar, M., & Franzson, H. (2007). Fracture pattern of Thjórsárdalur central volcano with respect to rift-jump and a migrating transform zone in South Iceland. Journal of structural geology, 29(5), 898-912.

Khodayar, M. (2013). Fracture Analysis from Aerial Imageries and Correlation with Triggered Earthquakes by Injection at Húsmuli, Hengill, South Iceland. Report Iceland GeoSurvey. Iceland GeoSurvey, Report íSOR-2013/008, 23.

Kristjánsson, B. R., Axelsson, G., Gunnarsson, G., Gunnarsson, I., & Óskarsson, F. (2016). Comprehensive tracer testing in the Hellisheidi Geothermal Field in SW-Iceland. In Proceedings, 41st Workshop on Geothermal Reservoir Engineering (Vol. 730).

Kristjánsdóttir,B. (2018) Seismic catalog, ISOR.

Loughlin, S. C. (2002). Facies analysis of proximal subglacial and proglacial volcaniclastic successions at the Eyjafjallajökull central volcano, southern Iceland. Geological Society, London, Special Publications, 202(1), 149-178.

Lund, B., & Slunga, R. (1999). Stress tensor inversion using detailed microearthquake information and stability constraints: Application to Ölfus in southwest Iceland. *Journal of Geophysical Research: Solid Earth*, *104*(B7), 14947-14964.

McGarr, A., Simpson, D., Seeber, L., & Lee, W. (2002). Case histories of induced and triggered seismicity. *International Geophysics Series*, *81*(A), 647-664.

Mildren, S., R. Hillis, P. Lyon, J. Meyer, D. Dewhurst and P. Boult (2005). FAST: A New Technique for Geomechanical Assessment of the Risk of Reactivation-related Breach of Fault Seals. AAPG Hedberg Series 2. 10.1306/1060757H23163.

Miller, A. D. (1996). *Seismic structure and earthquake focal mechanisms of the Hengill volcanic complex, SW Iceland* (Doctoral dissertation, Durham University).

Rinaldi, A. P. and Nespoli, M. (2017). TOUGH2-SEED: A coupled fluid flow and mechanical-stochastic approach to model injection-induced seismicity, Computer and Geosciences.

Ritz, V. A., Rinaldi, A. P., Castilla, R., Colas, E., Meier, P. M., Wiemer S., & COSEISMIQ team (2020). Preliminary Modelling Activities for an Adaptive Traffic Light System for the Hengill Geothermal Field. In Proceedings of world geothermal congress.

Sæmundsson, K. (1967). Outline of the structure of SW-Iceland. Visindafelag Islendinga.

Sæmundsson, K. (1995). Hengill Geological Map (Bedrock), 1: 50,000. *National Energy Authority, Reykjavík Municipal Heating and Iceland Geodetic Survey*.

Schorlemmer, D., Wiemer, S., & Wyss, M. (2005). Variations in earthquake-size distribution across different stress regimes. Nature, 437(7058), 539.

Scholz, C. H. (1998). Earthquakes and friction laws. Nature, 391(6662), 37.

Segall, P. (1989). Earthquakes triggered by fluid extraction. Geology, 17(10), 942-946.

Segall, P., Grasso, J. R., & Mossop, A. (1994). Poroelastic stressing and induced seismicity near the Lacq gas field, southwestern France. Journal of Geophysical Research: Solid Earth, 99(B8), 15423-15438.

Segall, P., & Lu, S. (2015). Injection-induced seismicity: Poroelastic and earthquake nucleation effects. Journal of Geophysical Research: Solid Earth, 120(7), 5082-5103.

Sibson, R. H. (1973). Interactions between temperature and pore-fluid pressure during earthquake faulting and a mechanism for partial or total stress relief. Nature Physical Science, 243(126), 66-68.

Sigmundsson, F., Einarsson, P., Rögnvaldsson, S. T., Foulger, G. R., Hodgkinson, K. M., & Thorbergsson, G. (1997). The 1994–1995 seismicity and deformation at the Hengill triple junction, Iceland: Triggering of earthquakes by minor magma injection in a zone of horizontal shear stress. *Journal of Geophysical Research: Solid Earth*, *102*(B7), 15151-15161.

Sigvaldason, G. E. (2002). Volcanic and tectonic processes coinciding with glaciation and crustal rebound: an early Holocene rhyolitic eruption in the Dyngjufjöll volcanic centre and the formation of the Askja caldera, north Iceland. Bulletin of Volcanology, 64(3-4), 192-205.

Tester, J. W., Anderson, B. J., Batchelor, A. S., Blackwell, D. D., DiPippo, R., Drake, E. M., ... & Petty, S. (2006). The future of geothermal energy. *Massachusetts Institute of Technology*, *358*.

Tómasdóttir, S. (2018). Flow Paths in the Húsmúli Reinjection Zone, Iceland.

Tryggvason, A., Rögnvaldsson, S. T., & Flóvenz, O. G. (2002). Three-dimensional imaging of the P-and S-wave velocity structure and earthquake locations beneath Southwest Iceland. *Geophysical Journal International*, *151*(3), 848-866.

Violay, M., Gibert, B., Mainprice, D., Evans, B., Dautria, J. M., Azais, P., & Pezard, P. (2012). An experimental study of the brittle-ductile transition of basalt at oceanic crust pressure and temperature conditions. Journal of Geophysical Research: Solid Earth, 117(B3).

8. Appendix

8.1. Available Data

Appendix 1: Data set available and sources

<table>
<tr><td rowspan="5">Seismicity</td><td colspan="2">Drilling phase</td><td>- SIL Catalog (1995-2018) - inaccurate localisations (depth)</td></tr>
<tr><td colspan="2">Injection Tests</td><td>- SIL Catalog (1995-2018) - inaccurate localisations (depth)</td></tr>
<tr><td rowspan="3">Injection phase</td><td>Sept. 2011 – Ap. 2012</td><td>- ISOR’s catalog (Sept. 2011 – April 2012) - accurate localisations</td></tr>
<tr><td>2012-2018</td><td>- SIL Catalog (1995-2018)</td></tr>
<tr><td>2018-2019</td><td>- 2018/2019 SED catalog</td></tr>
<tr><td rowspan="3">Structure</td><td colspan="2">Surface</td><td>- Aerial photography interpretation (ISOR, 2013)</td></tr>
<tr><td colspan="2">Wells</td><td>- HN-12, HN-14 and HN-16 (drilling report)
- Tracer tests (Kristjánsson et al., 2016)
- Permeable zone/Loss (Drilling report/excel file)</td></tr>
<tr><td colspan="2">Seismicity</td><td>- ISOR’s catalog (Sept. 2011 – Ap. 2011)</td></tr>
<tr><td rowspan="2">Stress field</td><td colspan="2">From focal Mechanisms</td><td>- Focal mechanisms (Sigríður Kristjánsdóttir, ISOR)</td></tr>
<tr><td colspan="2">From Well</td><td>- HN16 (Batir, 2012)</td></tr>
<tr><td>Temperature</td><td colspan="3">- Temperature model(Leapfrog model)
- Map of temperature (Helgadottir et al., 2010)</td></tr>
<tr><td>Hydraulique data</td><td colspan="3">– Injection data (Reykjavik Energy)
–
– Inflow (drilling report + Leapfrog model)
– Pressure data (Reykjavik Energy)
– Temperature of injected fluid - Graunhukar area (ISOR)</td></tr>
<tr><td>Geology</td><td colspan="3">– Geological log (Drilling report)
– Lithological model (Leapfrog Model)
– Bibliography</td></tr>
</table>

Appendix 2 : Data set available per well in Húsmúli area.

	HN-9	**HN-11**	**HN-12**	**HN-13**	**HN-14**	**HN-15**	**HN-16**	**HN-17**
Well Trajectory	x	x	x	x	x	x	X	x
Hydraulic data (active well)	x		x		x		X	X
Injection test					x	x		x
Inflow	x	x	x	x	x	x	x	x
Model tempetaure	x	x	x	x	x	x	x	X
Structure in well			x		x		x	
Stress field							x	
Geology (log)	x	x	x	x	x	x	x	x

Appendix 3: Table of analytic results of the bottom well pressure before and during injection. Pressure in bar.

Well id	**Water Table**	**Initial pressure (bottom well) 160°C**	**Injection pressure (160C°)**	**Injection pressure (bottom well) 140°C**	**Injection Pressure (bottom well) 120°C**
HN-09	250m	200.2	222.5	235.0	239.9
HN-12	280m	106.5	131.4	142.1	144.9
HN-14	230m	117.2	137.7	148.5	151.5
HN-16	270m	120.6	144.7	155.6	158.8
HN-17	270m	109.6	133.6	144.4	147.3

8.2. Geological context

Appendix 4: Aerial map of Reykjanes Peninsula with surface fracture orientations. Clifton and Kattenhorn (2006). In Hellisheidi area, the main trend is the N20-40° (yellow lines).

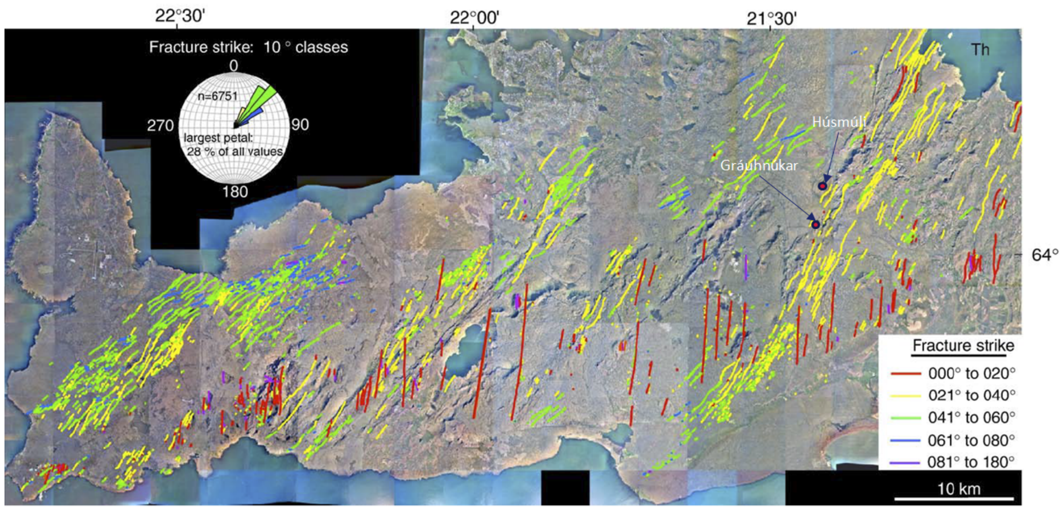

Appendix 5: Deformation in the transform zone of SISZ. A Riedel shear model of an E-W transform zone similar to SISZ and fracture types within the zone. R' : antithetic; R : Synthetic; PS : principal shear. (Khodayar and Franzson, 2007).

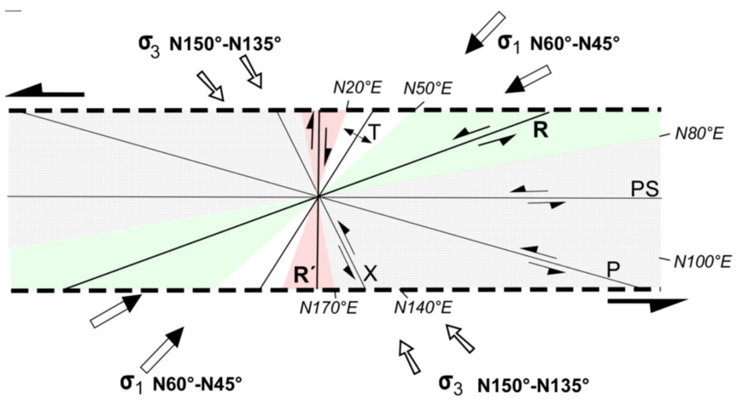

Appendix 6: 3D geological model highlighted the zone affected by the seismicity. Lithologic model is based on the Leapfrog© model of ISOR.

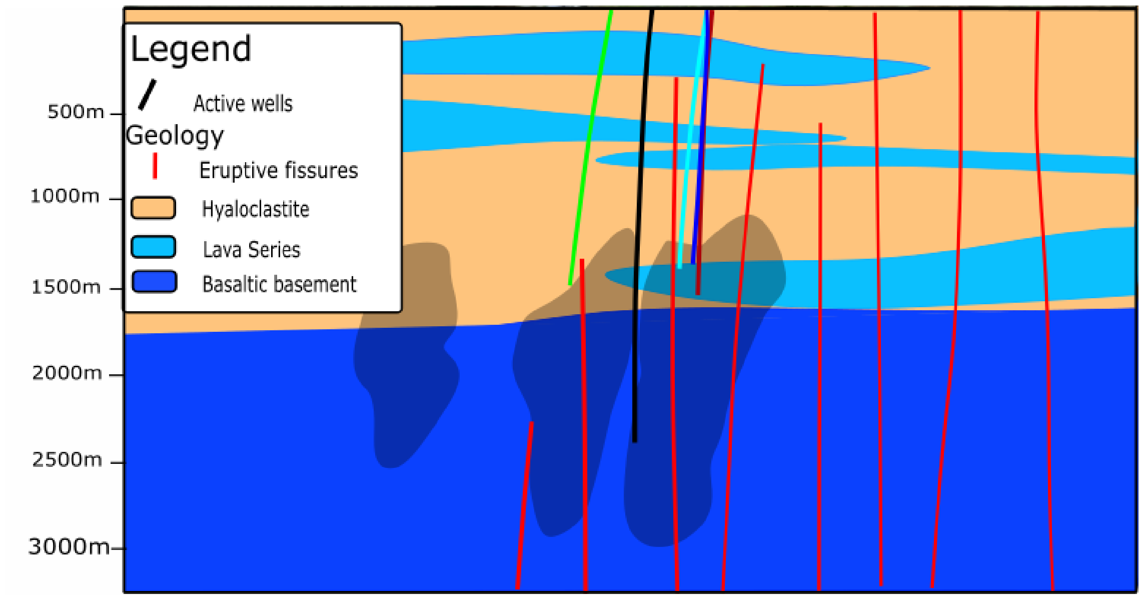

Appendix 7: Geological profile of the Húsmúli area with structures, permeable zones and lithologies

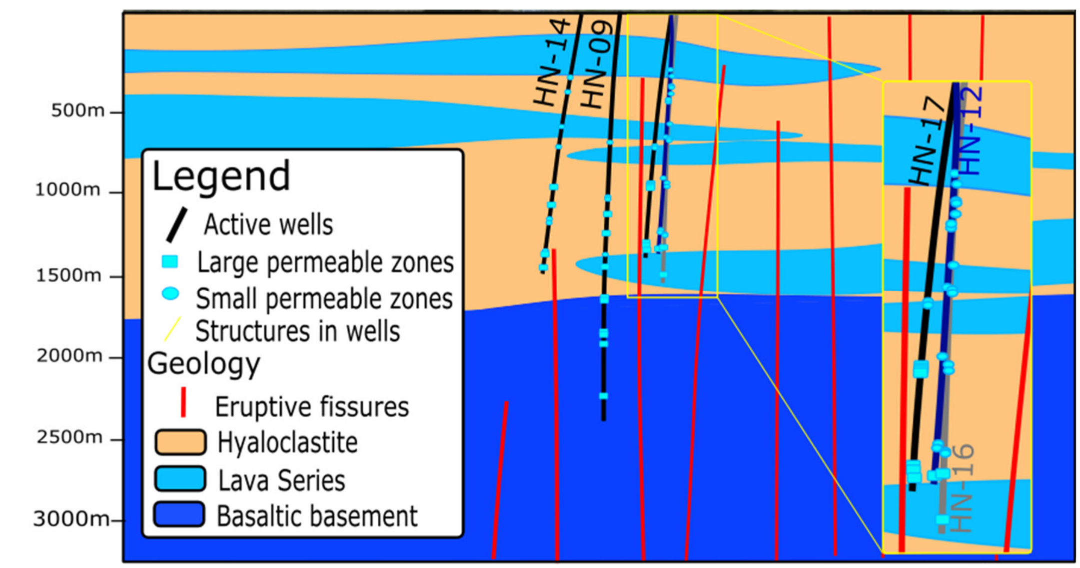

8.3. Evolution of the seismicity

Appendix 8: Evolution of the induced seismicity () and the injection rate in Húsmúli area (Seismic catalog: S. Kristjánsdóttir, 2018).

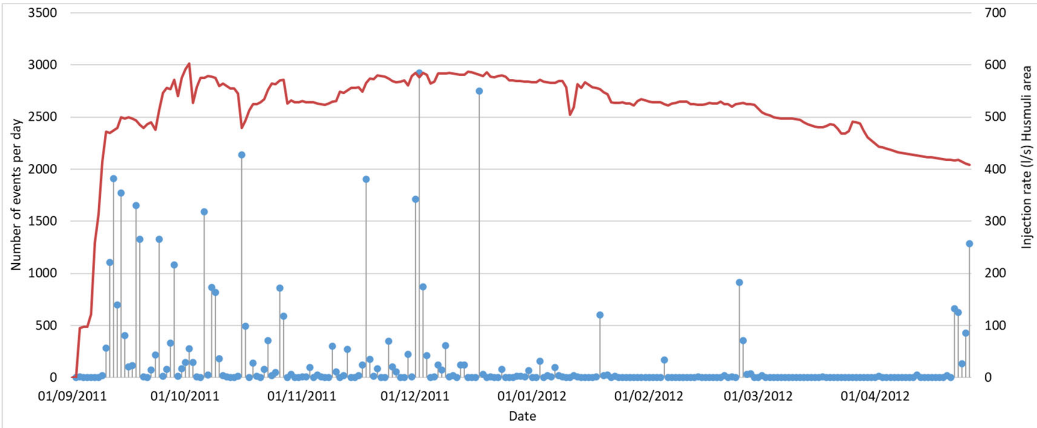

8.4. Structures

Appendix 9:Map showing the main transport of the tracer injected into well HN-9 (blue arrows) with indication of the travel time for each recovery well (Kristjánsson et al., 2016)

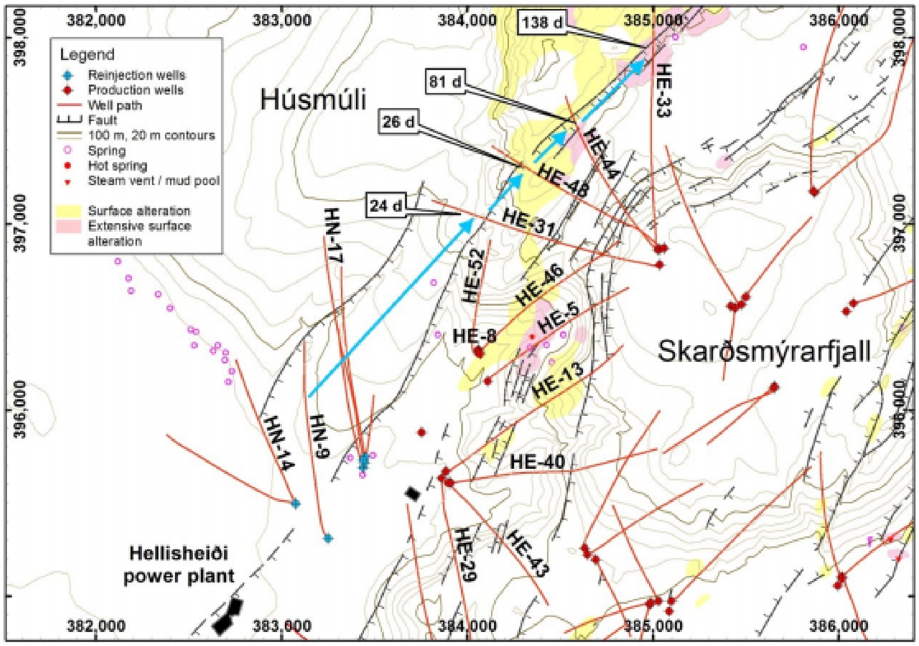

Appendix 10: Map showing the main transport of the tracer injected into well HN-8 (blue arrows) with indication of the travel time for each recovery well (Kristjánsson et al., 2016).

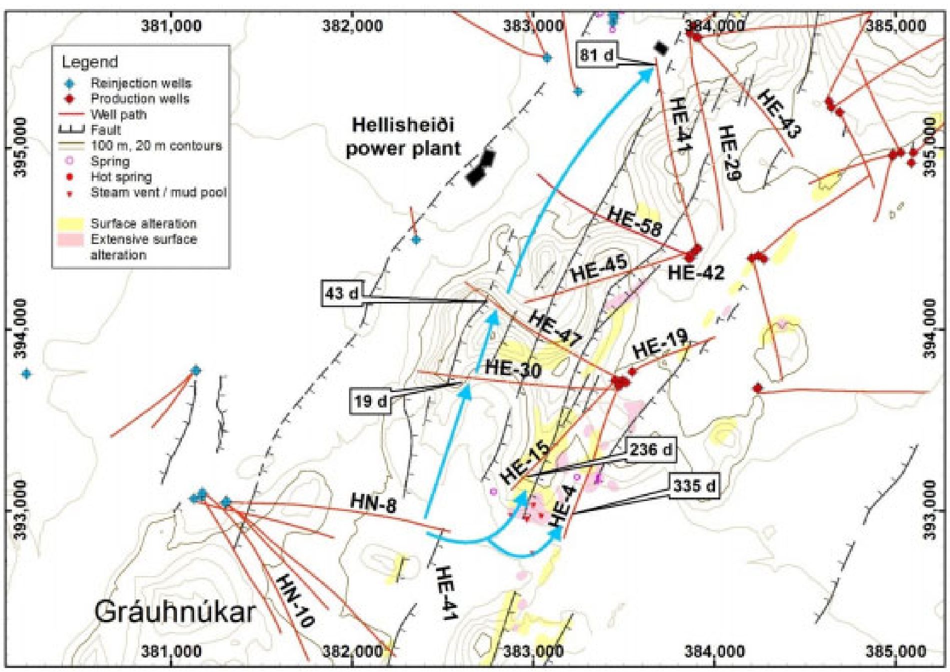

8.5. Stress

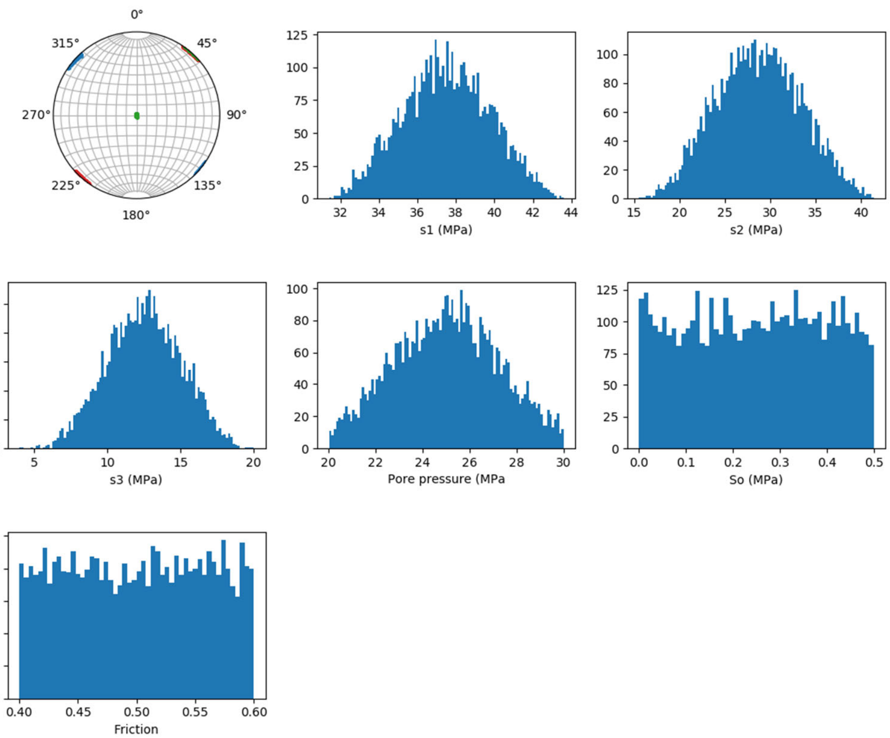

Appendix 11. Example of stress parameter sampling to estimate the reactivation potential of different fault orientations. 5000 realisations are run with truncated gaussian distributions for the stress parameters (orientations and magnitudes) and pore pressure. For the yield criteria (So=cohesion and friction coefficient), uniform distributions are used.

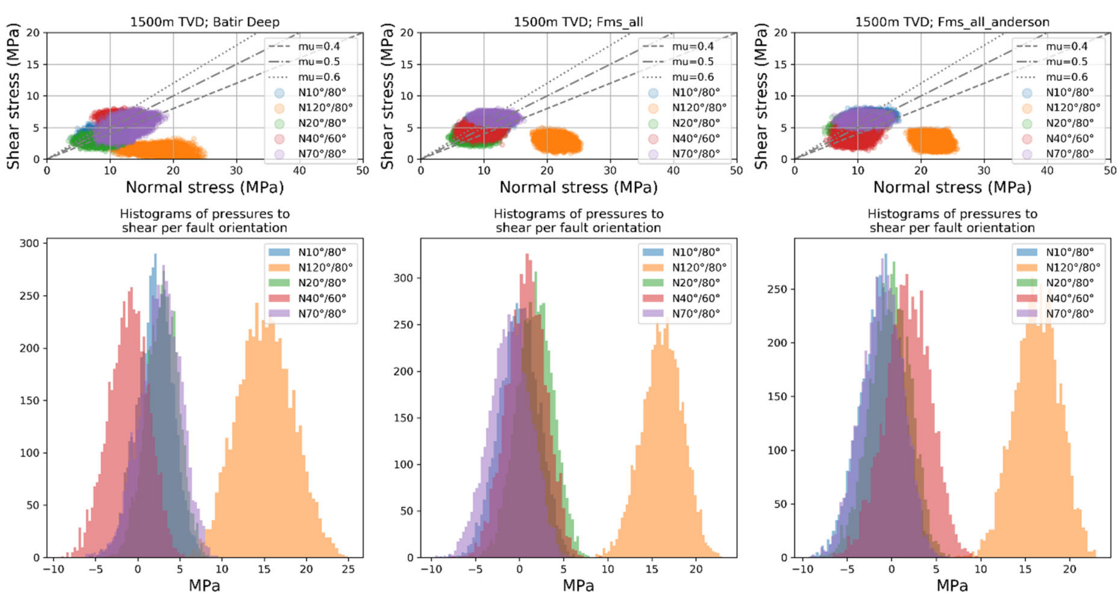

Appendix 12. Reactivation potential of main structural directions in the Húsmúli area for the 3 homogenous stress scenarios and a depth = 1500 mTVD.

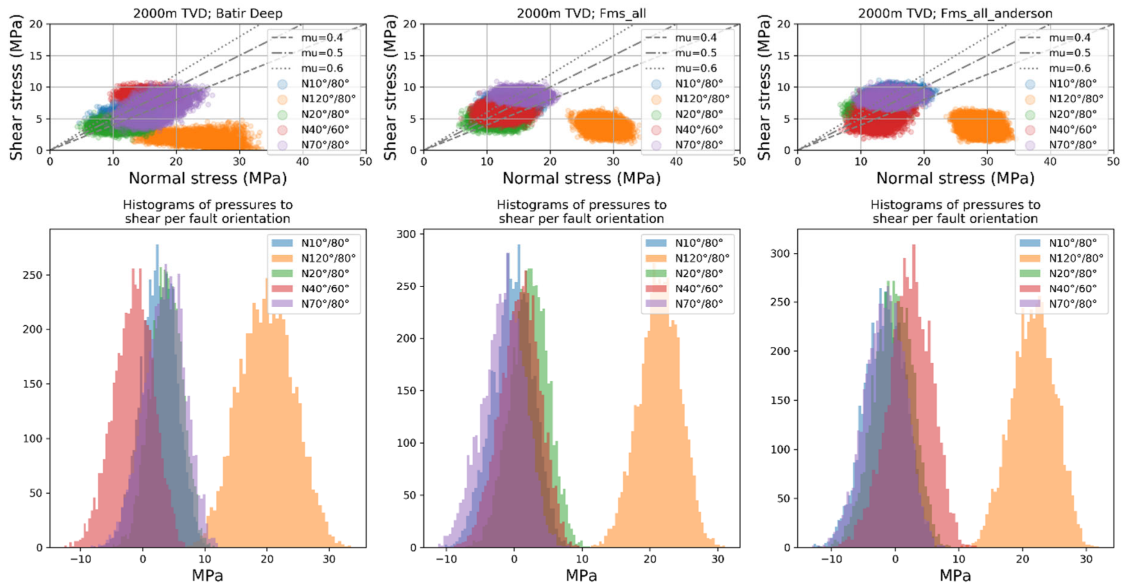

Appendix 13 Reactivation potential of main structural directions in the Húsmúli area for the 3 homogenous stress scenarios and a depth = 2000 mTVD.

8.6. Impact of the Temperature

Appendix 14: Diagram of the response to velocity changes and definition of the terms in the rate-state friction law. (Samuelson & Spiers, 2012).

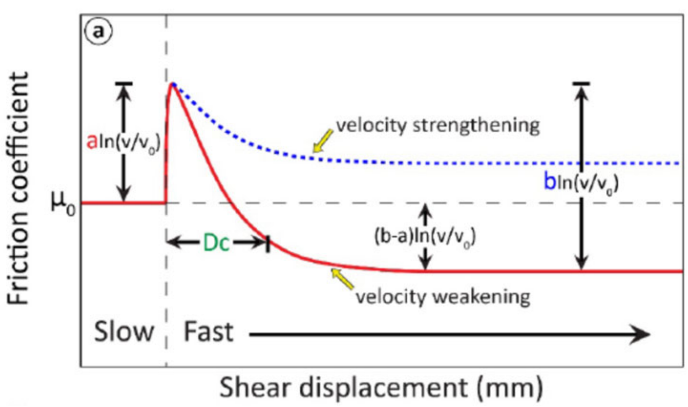

8.7. Hydraulic data

Appendix 15: Seismicity during the drilling for each well in Húsmúli.

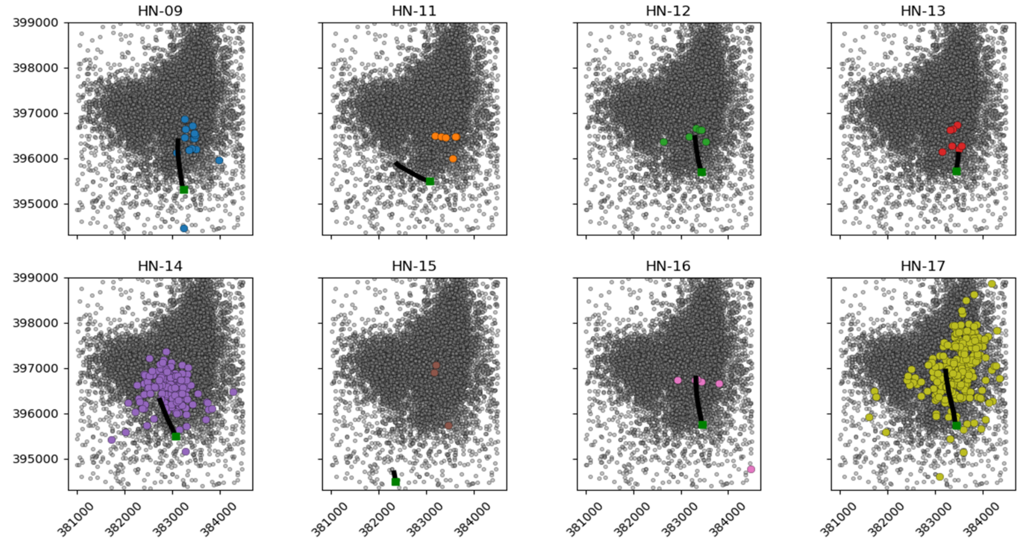

Appendix 16: Evolution of the total seismicity and the injectivity in time for the well HN-17 (Húsmúli).

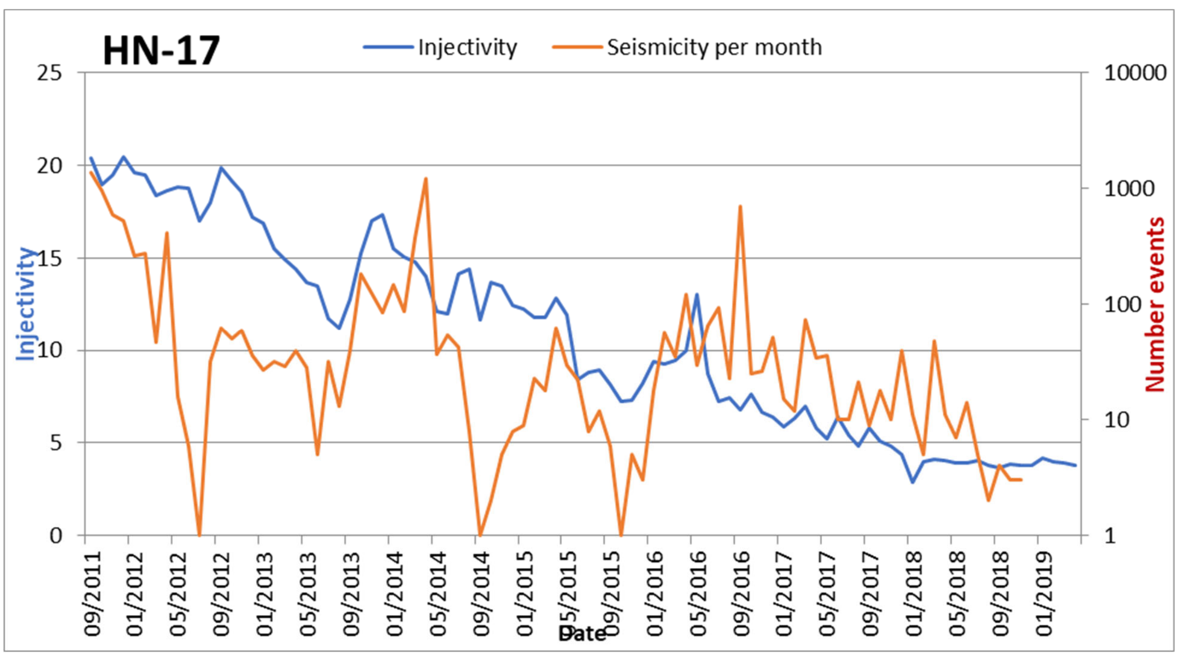

Appendix 17: Seismicity during drilling of well HN-17 in the Húsmúli Area. The magnitude (Ml) and cumulated number of events (Ntot) as measured by the national seismological network are shown. (Gunnarsson et al., 2015).

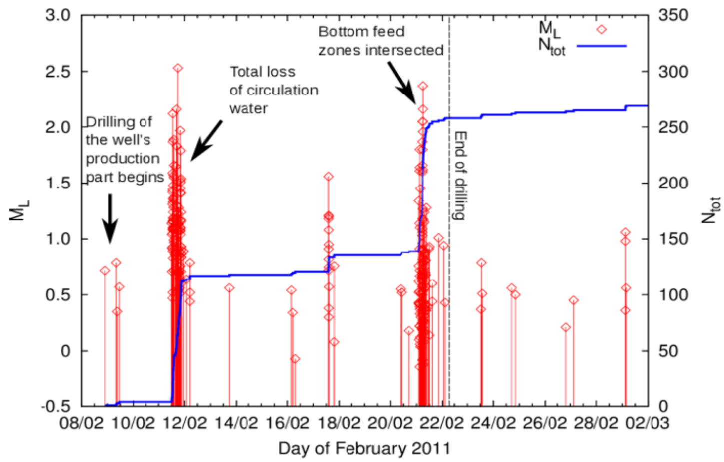

8.8. Impact of the injection

Appendix 18: Influence of the injection rate on the number of seismic events. Correlation per months (SIL Catalog)

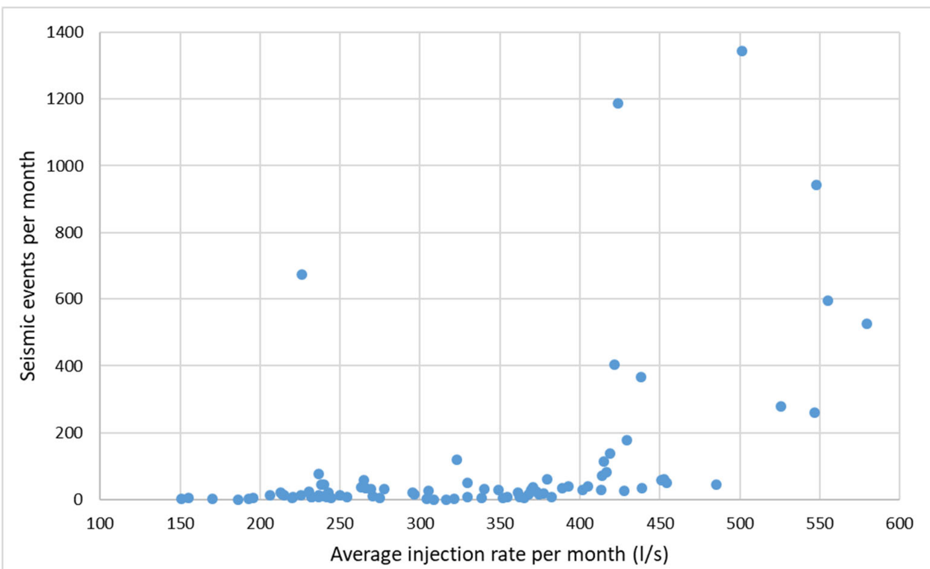

Appendix 19: Influence of the injection rate on the number of seismic events. Correlation per six months (SIL Catalog)

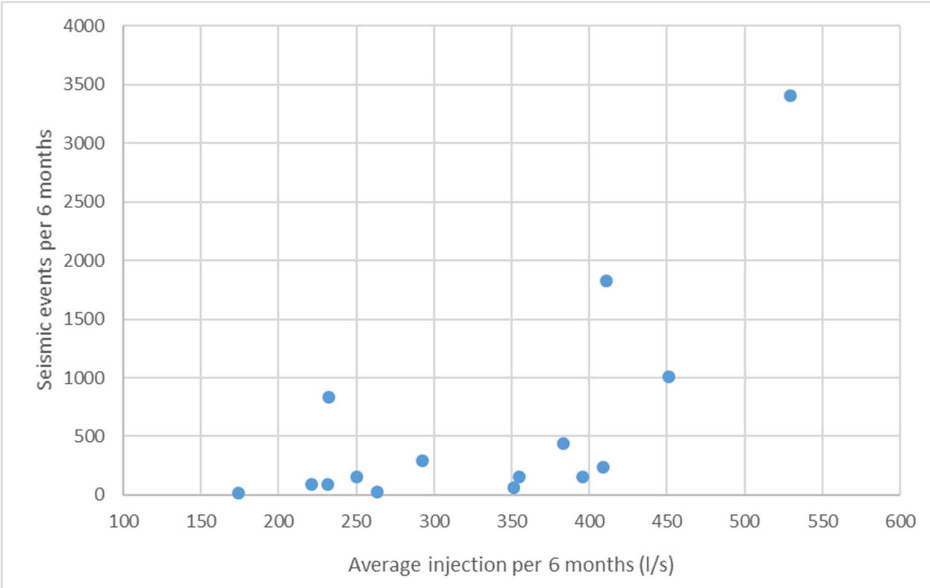

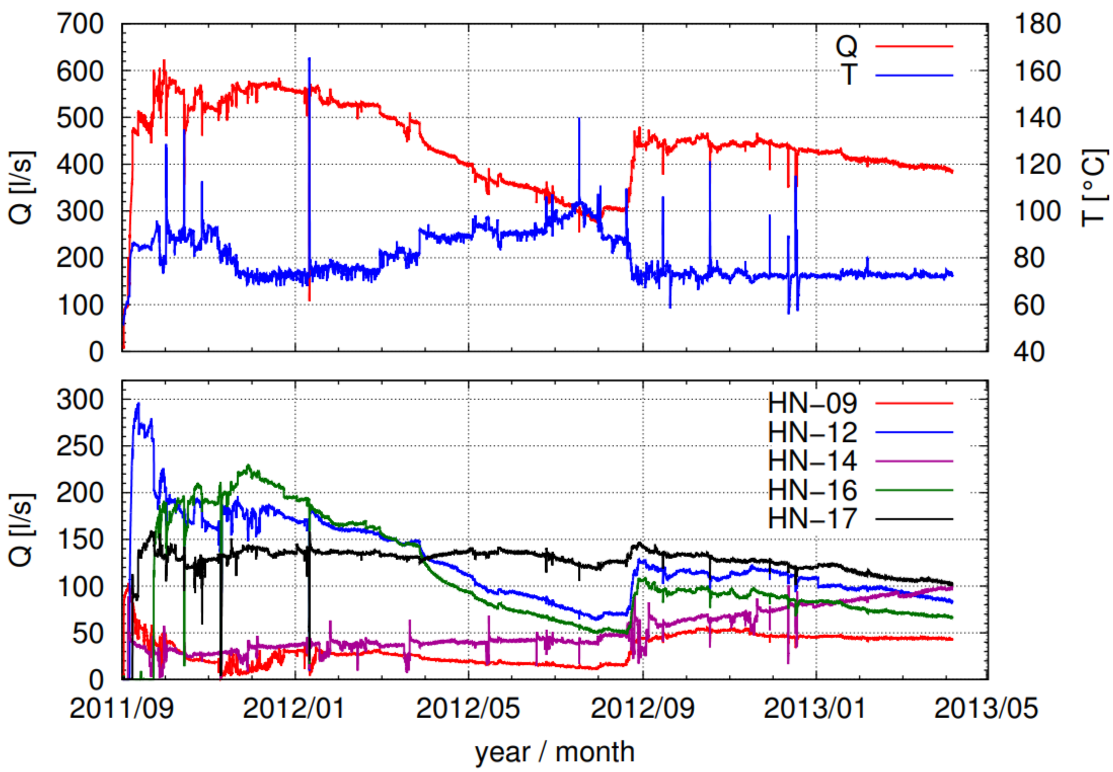

Figure 39: Upper graph: Total flow (Q) in to the Húsmúli reinjection zone and the temperature (T) of the injected water from the commission of the zone in September 2011 till middle of April 2012. Lower graph: Flows (Q) into individual wells. Time scale is the same for both graphs (Gunnarsson, 2013).